University of Alberta

Gelatin as a Target Medium for Ballistic Sizing of Aerosol Particles

by

James E. Barth

A thesis submitted to the Faculty of Graduate Studies and Research
in partial fulfillment of the requirements for the degree of

Master of Science

Department of Mechanical Engineering

Edmonton, Alberta
Spring 2007

Library and Archives Canada

Published Heritage Branch

395 Wellington Street
Ottawa ON K1A 0N4
Canada

Bibliothèque et Archives Canada

Direction du Patrimoine de l'édition

395, rue Wellington
Ottawa ON K1A 0N4
Canada

Your file Votre référence
ISBN: 978-0-494-29936-4
Our file Notre référence
ISBN: 978-0-494-29936-4

NOTICE:
The author has granted a non-exclusive license allowing Library and Archives Canada to reproduce, publish, archive, preserve, conserve, communicate to the public by telecommunication or on the Internet, loan, distribute and sell theses worldwide, for commercial or non-commercial purposes, in microform, paper, electronic and/or any other formats.

The author retains copyright ownership and moral rights in this thesis. Neither the thesis nor substantial extracts from it may be printed or otherwise reproduced without the author's permission.

AVIS:
L'auteur a accordé une licence non exclusive permettant à la Bibliothèque et Archives Canada de reproduire, publier, archiver, sauvegarder, conserver, transmettre au public par télécommunication ou par l'Internet, prêter, distribuer et vendre des thèses partout dans le monde, à des fins commerciales ou autres, sur support microforme, papier, électronique et/ou autres formats.

L'auteur conserve la propriété du droit d'auteur et des droits moraux qui protège cette thèse. Ni la thèse ni des extraits substantiels de celle-ci ne doivent être imprimés ou autrement reproduits sans son autorisation.

In compliance with the Canadian Privacy Act some supporting forms may have been removed from this thesis.

While these forms may be included in the document page count, their removal does not represent any loss of content from the thesis.

Conformément à la loi canadienne sur la protection de la vie privée, quelques formulaires secondaires ont été enlevés de cette thèse.

Bien que ces formulaires aient inclus dans la pagination, il n'y aura aucun contenu manquant.

Canada

To my family, my girlfriend, and my friends: You supported me, kept me sane, and believed in me when I couldn't believe in myself. Without you, this would never have come to pass. I love you all.

Abstract

Ballistic sizing of aerosol particles offers a novel solution to the unique constraints imposed by the possibility of in-situ particle measurement in remote (and extra planetary) environments. Initial theoretical considerations predicted that an appropriate material would allow for impacting aerosol particles to a measurable and predictable depth in the ballistic target. Low-concentration gelatin was investigated as a possible target medium that may allow for ballistic behavior for the low kinetic energies associated with aerosols. Highly monodisperse polymer resin particles were entrained in an air stream of measured velocity, and fired into 2% gelatin targets in ambient conditions. It was discovered that the ballistic behavior was negligible, possibly due in part to the effects caused by high target surface deflection under the application of the particle laden air jet. Therefore, low concentration gelatin would appear to be unsuitable for ballistic particle sizing, though there may be other suitable target media.

Acknowledgements

I would like to thank my supervisor, Dr. Warren H. Finlay, for his invaluable guidance and support throughout the completion of this thesis. Also, many thanks to Helena Orszanska and Biljana Grgic of the Aerosol Research Laboratory of Alberta, and Rakesh Bhatnagar of the University of Alberta Advanced Microscopy Unit, for their time, expertise, and assistance throughout my endeavor. Finally, I offer my grateful acknowledgement to the Natural Sciences and Engineering Research Council of Canada, for their generous financial support of my research.

Table of Contents

Chapter 1 - Introduction p.1

1.1 - Preamble p.1

1.2 - Reason for Study p.2

1.3 - Scope of Investigation p.3

Chapter 2 - Theory p.4

2.1 - Ballistic Penetration Theory p.4

2.2 - Particle Motion Prior to Impact p.9

2.2.1 - Axisymmetric, Impinging Turbulent Jets p.9

2.2.2 - Aerodynamic Focusing p.12

2.2.3 - Deformation of the Target Surface p.12

2.3 - Revised Prediction of Particle Penetration p.14

Chapter 3 - Experimental Design p.15

3.1 - Target and Particle Material Selection p.15

3.1.1 - Impact Medium p.15

3.1.2 - Particle Material p.17

3.2 - A Tensile Specimen for Measuring Gelatin Strength p.18

3.3 - Modeling Extreme Conditions p.19

3.4 - Measuring Particle Speed p.21

3.4.1 - Estimation of Particle Velocity in Vacuum Chamber p.22

3.4.2 - Particle Image Velocimetry p.23

3.4.3 - Laser Doppler Anemometry p.24

3.5 - Measuring Particle Penetration Depth p.26

3.5.1 - X-Ray Imaging p.26

3.5.2 - Confocal Microscopy p.27

3.6 - Overall Apparatus p.30
3.6.1 - Gelatin Concentration and Target Specimen Shape p.30
3.6.2 - Particle Firing and Deaggregation p.31
3.6.3 - Complete Apparatus p.35

Chapter 4 - Results p.37
4.1 - Gelatin Tensile Strength p.37
4.2 - Particle Penetration Depth Measurements p.38
4.3 - Particle Velocity Measurements p.43

Chapter 5 - Discussion p.44
5.1 - Measurement Accuracy p.44
5.1.1 - Gelatin Tensile Strength p.44
5.1.2 - Velocity Measurements p.47
5.1.3 - Particle Penetration Depth p.48
5.2 - Examination of Results p.49
5.3 - Comparison to Theory p.55
5.3.1 - Possible Unconsidered Penetration Mechanisms p.56
5.3.2 - Possible Amendments to Theory p.58

Chapter 6 - Conclusions and Recommendations p.62
6.1 - Conclusions p.62
6.2 - Recommendations p.63

Bibliography p.65

Appendix A - Matlab Image Processing Code p.67
Appendix B - Raw Data p.72
Appendix C - Derivations p.76
C.1 - Stored Elastic Energy Due to Surface Deformation p.76
C.2 - Frictional Force Acting on a Spherical Particle p.77

List of Figures and Tables

Figures

Figure 2.1:	Geometry of the Ballistic Penetration Model	p.4
Figure 2.2:	Predicted Depth of Penetration of Aerosol Sized Particles	p.8
Figure 2.3:	Schematic of Impinging Jet Flow Streamlines, Showing Different Flow Zones	p.10
Figure 2.4:	Schematic of a Vector Normal to the Deformed Target Surface	p.13
Figure 2.5:	A comparison of predicted penetration before and after aerodynamic effects are taken into account	p.14
Figure 3.1:	Regular, and 'Exploded' Views of the Tensile Specimen Mould	p.18
Figure 3.2:	Cross Section of Gelatin Tensile Specimen Perpendicular to Plate Surfaces	p.19
Figure 3.3:	Vacuum Chamber Apparatus	p.21
Figure 3.4:	Top View of the Probe Volume, With an Arrow Showing Direction of Particle Motion	p.24
Figure 3.5:	Illustration of Pinhole Filtering Out-of-Plane Light	p.28
Figure 3.6:	Cross Section View of Petri Dish (Courtesy of Electron Microscopy Science's Website)	p.30
Figure 3.7:	Top View of a Plastic Valve when a) Closed, and b) Opened	p.32
Figure 3.8:	Particle Firing Assembly, Showing Internal Geometry	p.33
Figure 3.9:	Schematic of Cone Attached to Particle Firing Assembly	p.34
Figure 3.10:	Schematic of Complete Particle Firing Apparatus Left: Top View. Right: Front View.	p.35
Figure 4.1:	a) A sample of cross sections near the surface, and b) Near the bottom of the particle field. Green Fluorescence is shown on the left, Red on the right.	p.39
Figure 4.2:	A plot of particle center location distribution for a series of gelatin section images	p.41
Figure 4.3:	a) Schematic of how the specimen was viewed, b) Transmission image of the section, c) Fluorescing Image from a plane within the specimen	p.42
Figure 5.1:	Fluorescent image of a single focal plane from a sectioned gel target	p.49
Figure 5.2:	Transmission Microscope image of the sectioned gel target	p.52
Figure 5.3:	Schematic of range of estimated particle depth positions	p.54

Figure 5.4: Predicted Range of Penetration for varying Physical Properties p.55
Figure 5.5: Contact Geometry Prior to Rupture p.58

Figure 6.1: Schematic of a Piston Ram Particle Firing System p.63

Figure B.1: Graphical Output for Penetration Depths of Experiment LPV3 p.73
Figure B.2: Graphical Output for Penetration Depths of Experiment LPV4 p.74

Figure C.1: Gel Elastic Deformation due to Particle Impact p.76
Figure C.2: Particle Schematic for Frictional Force Derivation p.77

Tables

Table 5.1: Average Values of Data from Laser Doppler Anemometer p.47
Table 5.2: Potential Elastic Energy Stored for a Given Contact Angle p.59

Table B.1: Velocity Measurements Taken with LDA p.72
Table B.2: Penetration Depth Data Taken From Program Output p.75

List of Symbols

Roman Letters

a	Flow strength
C_c	Cunningham Slip Correction Factor
d	Penetration Depth
d_P	Particle Diameter
D	Flow Diameter (Stokes Number)
F_D	Fluid drag force acting on a particle
F_f	Frictional Force acting on a particle
F_N	Normal Force acting on a particle
h	Deformation height of gelatin in frictional derivation
k	Effective spring constant of the gelatin
r	Particle radius
R_{plate}	Radius of Collecting Surface
s	Depth gelatin surface is deformed to by particle impact
Stk	Stokes Number
U	Total elastic energy stored in compressed gelatin surface
U_o	External Velocity in Stokes Flow Equation
V	Particle Velocity
V_{impact}	Particle Impact Velocity
V_∞	Mean Jet Freestream Velocity

Greek Letters

$\Delta\sigma_T$	Error in measured tensile yield strength
λ	Mean Free Path of Molecules in Air
μ	Viscosity
μ_k	Coefficient of kinetic friction
ρ_P	Particle density
ρ_t	Target density
σ_y	Target yield strength
θ	Angle of contact

Chapter 1

Introduction

1.1 - Preamble

There are numerous methods and technologies for the measurement of fine particle size distribution in aerosols and dusts, ranging from cascade impactors, to light scattering, to laser detectors. All of these are well suited to finding important particle parameters such as mass mean diameter in a laboratory or industrial setting.

However, outside of these settings, the utility of these methods can be greatly diminished. If one is interested in making in-situ particle size data collection in remote, inaccessible places and environments, these systems can run into problems with energy supply, size, and ease of transport. Additionally, sensitive components may break down easily in the environmental conditions they are exposed to. A large desert (for finding an unbiased sample of particle size in a dust storm), or even more extreme, the rarefied atmosphere of Mars, are just two examples where such problems could be encountered.

Of all the planets in our solar system, Mars is probably one of the most intensely studied planets after our own. Few planets seem to have captured the popular imagination like the "Red Planet" has, and fascination with it continues unabated, some nations even announcing intention of eventually sending manned missions there one day.

A study of Martian dust characteristics could provide useful information. Such a study could provide information on the climate of Mars, and give new insight into the

weather patterns observed, including massive dust storms and "dust devils" which commonly occur on the planet. Martian dust could also provide clues about the surface and terrain of Mars, or even give hints to possible hazards that a future manned mission to Mars could face. For example, fine Mars dust could have negative physiological effects on humans if it found its way into the respiratory tract, perhaps in a similar fashion to the allergic reaction to moon dust that Apollo 17 astronaut Harrison Schmitt experienced, or to illness experienced by workers that have inhaled dust of similar composition to Mars dust.

1.2 – Reason for Study

For all the potential benefits of studying atmospheric dust in environments as harsh and remote as Mars, there are severe constraints on which types of particle sizing equipment could be used. An appropriate system would have to provide an unbiased measurement of particle size distribution while being small and lightweight, require low power consumption, be robust enough to withstand the conditions it will face, be capable of remote operation and data transmission, and finally, be of a reasonably low cost as retrieval of the system may be impossible following deployment. To the author's knowledge, there is no exiting instrumentation package that fulfills these criteria.

This thesis was concerned with the proof of concept of a type of aerosol particle sampling system which may fit within the necessary constraints for a small, remotely operated system. Specifically, it was decided to examine if it were possible to sample and size aerosol size particulate matter with a ballistic impact device. Ballistic impact

mechanisms are already in use in fields such as forensics and the recently completed Stardust mission that was conducted by NASA.

1.3 – Scope of Investigation

To narrow the focus of what could potentially be a rather broad study, it was decided to choose a set of parameters to fulfill the 'proof of concept' for a ballistic aerosol size sampler.

The experiment focused on a single target material, under a single set of conditions. This material was to be chosen to be easy to produce, cheap, have consistent physical properties, and allow for predictable, repeatable particle penetration characteristics. It was further decided that a range of monodisperse particles of known diameter would be fired at the target material. Particle speed would be measured in order to determine the correlation between particle size and momentum versus the depth the particles penetrate into the target medium.

Chapter 2

Theory

2.1 - Ballistic Penetration Theory

There has been a great deal of experimental work done on examining the interactions between a projectile and the target it penetrates, which have allowed for the build up of a theoretical model of penetration.

To begin, the positive direction of motion is defined as being normal into the target surface; that is, for theoretical considerations, the particle's motion is perpendicular to the surface of the target at impact, as is shown in Figure 2.1.

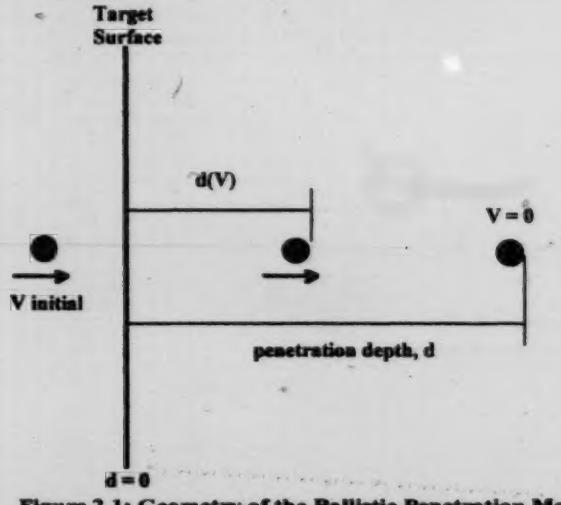

Figure 2.1: Geometry of the Ballistic Penetration Model

The coordinate origin is located at the target surface. Thus, according to Newton's second law:

$$\frac{d}{dt}(mV) = -F, \quad (1)$$

or, the change of the projectile's momentum with time is due to the net resistive force acting against the particle.

This resistive force can be attributed to three major components: a resistive inertial force of the target material, a target yield force, and a frictional resistive force. It has been suggested that the total force acting on the particle is of the form

$$F = a + bV + cV^2, \quad (2)$$

where a, b and c are constants related to the yield force, frictional force, and inertial resistive force respectively. (Dehn, 1986)

It was noted by Dehn that the mean pressure exerted by a target on the projectile at the surface is roughly three times the yield strength of the target. Therefore, the first constant was defined as

$$a = 3A\sigma_y, \quad (3)$$

the observed mean pressure multiplied by the frontal area of the projectile.

The target inertial resistive force would be an energy dissipated per unit volume (or force per unit area) of the yielding target material ahead of the projectile, and so this term would take the form

$$cV^2 = 0.5\rho_t AV^2. \quad (4)$$

The frictional term would be a term showing dissipation of heat through the physical mechanisms of frictional retardation of the particle. However, it has been shown that for most cases, the target cannot safely absorb all the heat dissipated, and so a thin film of fluid often forms around the edges of the particle. In this case, the frictional forces acting on the particle may be very small in relation to the other two forces, perhaps

contributing a maximum 3% of the total energy dissipation in the process. (Awerbuch, 1970)

Therefore, considering the second term in (2) to be negligible in relation to the other two, substituting (2), (3), and (4) back into (1) yields the formula

$$\frac{d}{dt}(mV) = -\left(3A\sigma_y + 0.5\rho_t AV^2\right). \tag{5}$$

To solve this equation, first examine the left-hand side term. For this experiment, the particles fired at the target should not gain or lose mass, and will be spherical in shape.

Therefore, the mass term may be moved out of the differential, giving

$$m\frac{dV}{dt} = -\left(3A\sigma_y + 0.5\rho_t AV^2\right), \tag{6}$$

with m defined by the particle's volume and density as

$$m = \frac{4\pi r_P^3}{3}\rho_P. \tag{7}$$

Finally, manipulating the velocity differential, penetration depth (or distance in the x-direction) may be solved for as a function of impact velocity. In order to do this, it is necessary to recognize that

$$\frac{dV}{dt} = \frac{dV}{dx}\frac{dx}{dt} = V\frac{dV}{dx}. \tag{8}$$

Substituting (7) and (8) into (6), the final form

$$V\frac{dV}{dx} = -\frac{3}{4r_P\rho_P}\left(3\sigma_y + 0.5\rho_t V^2\right), \tag{9}$$

is obtained. This may be rearranged and integrated with a boundary condition of penetration depth being zero for zero initial penetration velocity

$$d(V = 0) = 0, \tag{10}$$

to get the final theoretical depth of particle penetration based on impact velocity, which is

$$d = \frac{4r_p\rho_p}{3\rho_t}\left[\ln\left(0.5\rho_t V_{impact}^2 + 3\sigma_y\right) - \ln\left(3\sigma_y\right)\right]. \quad (11)$$

It should be noted that since this equation was derived with the target surface as the origin, with a particle of known velocity initially just touching the surface with its leading edge, this depth is the final location of the particle's leading edge. In this case, the deepest surface of the sphere is what the predicted depth signifies.

There is room for some error in this derivation: neglecting the frictional forces will obviously introduce some error into the model, and the target may have significant elasticity. However, the elasticity may be already incorporated into the model when measurements of the target yield strength are made, and the elastic properties may also be insignificant compared to the kinetic energy of the particle. Certainly, the model has shown good agreement with depth of penetration into human skin for a range of particle sizes with velocities ranging from a Mach number of 0.5 to supersonic. (Mitchell et al., 2003) As human skin is itself highly elastic, it seems reasonable that any target medium chosen for these experiments ought to also show agreement with theory.

With this model, one can therefore predict the depth of penetration of aerosol-sized particles given a reasonable estimate of particle and target properties, and impact velocity. For a sample calculation, it was assumed that the target was a porous material with a density roughly 95% that of water, the particles were of a polymer resin with a density 1.5 times that of water, and that the particles were moving at 75 m/s. The target tensile strength was estimated to be 2 kPa. The results are shown in Figure 2.2 below.

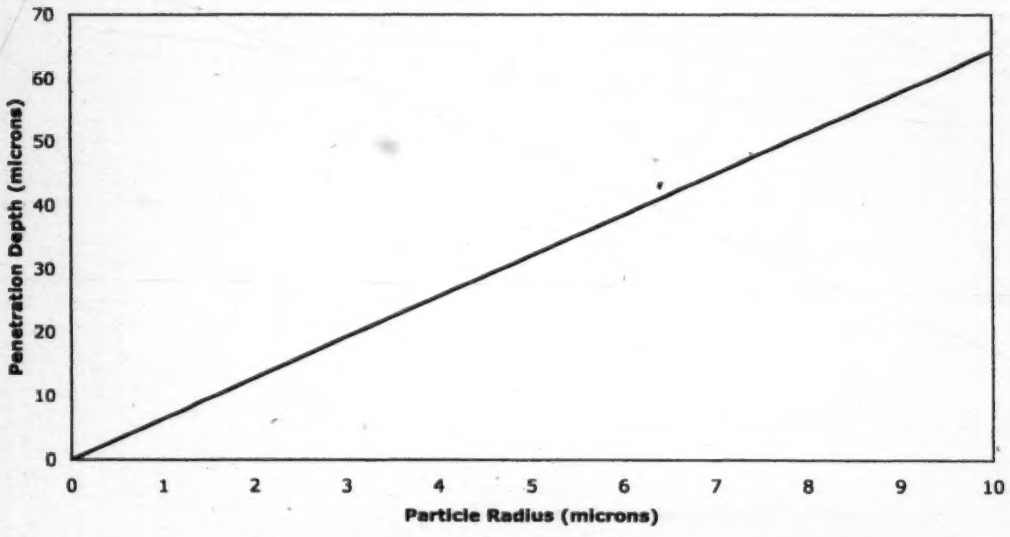

Figure 2.2: Predicted Depth of Penetration of Aerosol Sized Particles

Figure 2.2 is the estimated penetration depth for spherical particles that are 10μm or less in diameter. As can be seen, with all other parameters fixed at the values given above, depth of penetration was predicted to be about 6.4 times the diameter of the particle. This difference in penetration depths for different sizes of particles is the behavior could possibly be exploited as a method for cheaply sizing particles.

The parameters used to generate Figure 2.2 were assumed to be of reasonable values. Certainly, wind speeds on earth rarely reach 75 m/s, but wind speeds on Mars can easily be as high as tens of meters per second, so this velocity is a reasonable estimate. The target density and strength were estimated based on the fact that porous media, even those constituted of relatively heavy molecules will contain significant fractions of open space, and any material that would allow for ballistic behaviors at such low energies as aerosol particles would collide with must have a rather low tensile strength.

Finally, the particle density was estimated on the assumption that any particles that could be acquired with a suitable level of monodispersity would be likely made of a polymer material.

Given the above, it seems as though it should be possible to remotely size particles with a ballistic impact apparatus, provided the proper target material is found.

2.2 – Particle Motion Prior to Impact

In order to accelerate particles to the velocity at which they impact, it was decided early on that the best way in which to bring the particles up to speed was to entrain them within a stream of air moving at known velocity, which could then be directed onto the target. This type of flow is commonly referred to as impinging jet flow.

2.2.1 – Axisymmetric, Impinging Turbulent Jets

The impingement of a jet onto a planar surface has great practical value both in heat and mass transfer applications, and as such has been the subject of much investigation both experimentally and numerically.

An impinging jet can be considered as four distinct zones, according to Jambunathan et al. (1992). These zones are the initial mixing zone, the established zone, the deflection zone, and the wall jet. (See Figure 2.3) A turbulent jet will exit the nozzle in a nearly 'plug' flow, and will expand as it entrains quiescent fluid from the surroundings, gradually losing its radial plug velocity profile until the jet no longer contains a region of constant axial velocity on average. This zone is the initial mixing

zone, and is followed immediately by the established zone, in which the jet will continue to expand radially.

As the jet approaches the planar surface, the flow enters the deflection zone, in which boundary layer effects occur, and the flow streamlines are forced to diverge from the jet's axial direction. The boundary layer effects are dominant, and the flow is eventually forced parallel to the plates, which is where the wall jet begins.

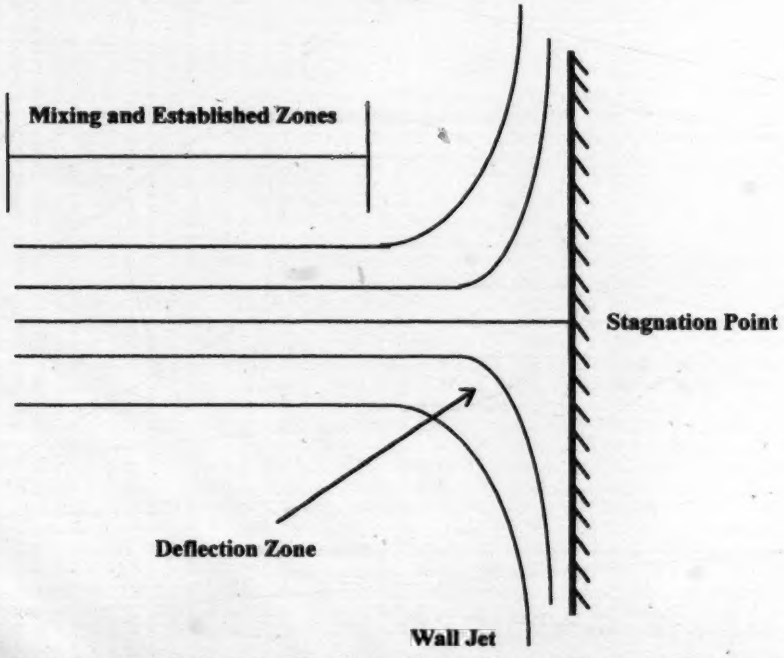

Figure 2.3: Schematic of Impinging Jet Flow Streamlines, Showing Different Flow Zones

The region of greatest interest for this study was the deflection zone. In this region, particles traveling at high speed would have too much inertia to be able to follow the path of the diverging streamlines, and if possessing enough inertia, could slip through the boundary layer and impact on the surface. This region has undergone some study for particle laden flows and surface deposition, however to the author's knowledge, these have been for rigid plates that typically cause impacting particles near the jet axis to rebound from the surface. (Anderson and Longmire, 1995; Burwash et al., 2006)

Experimental measurements of the axial velocity of an impinging turbulent jet have shown that as the flow approaches the stagnation point, the average peak velocity can be as low as 50% of the initial axial velocity when the flow is roughly one tenth of the jet's initial diameter from the surface. (Fairweather and Hargrave, 2002) As these measurements were made on micron sized particles using particle image velocimetry, it seems reasonable to assume that smaller particles fired in a stream of air would be more likely to follow the flow streamlines at sufficiently low speeds. Larger particles, and particles traveling at higher speeds would be more likely to show inertial effects.

Particles that continue on towards the surface but do not follow streamlines would rely on their inertia to pass through the surface flow boundary layer and impact on the surface. The parameter of use in predicting whether or not a particle has sufficient inertia to break free of flow streamlines and impact on the plate is known as Stokes Number,

$$Stk = \frac{U_o \rho_P d_P^2 C_c}{18 \mu D}. \tag{12}$$

C_c is the Cunningham Slip Correction factor, used for determining the effects of having particles close to the mean free path of air molecules, and is defined as

$$C_c = 1 + 2.52 \frac{\lambda}{d_P}, \tag{13}$$

where λ is the mean free path of air molecules (0.067 μm at room temperature.)

Generally, if a particle has a Stokes Number greater than or equal to 1, it will move relative to the fluid streamlines in the case of a rapid change of direction. (Finlay, 2001) A 10.6 micron particle entrained in a jet flow initially at 40 m/s and 5 mm in diameter has a Stokes number of roughly 4, and would therefore be expected to impact on the wall.

2.2.2 – Aerodynamic Focusing

Given the above discussion, it seems most likely that the particles which will retain enough axial velocity to penetrate the target medium will be those which remain nearer to the core of the jet as it enters the flow deflection zone near the target surface. Particles which are entrained in the outer edges of the expanding jet will likely lose sufficient velocity such that they will follow the flow streamlines more closely, and therefore only impact the surface due to sedimentation effects, and then only if the flow is vertical downward onto the target surface.

However, it is possible to ensure that as many particles in the air stream as possible will stay near the jet core by having the jet exit from a converging nozzle. It has been shown that for particle laden flows with flow Reynolds numbers as low as 15 and extending well into the supersonic range, that as particles entrained in the flow exit the nozzle, they will retain some radially inward component of velocity. (Rao et al., 1993) It is therefore reasonable to assume that the particles in the jet would remain roughly in the same radial distance relative to the jet axis for the duration of flight from the nozzle, to the impact target.

2.2.3 – Deformation of the Target Surface

A sufficiently high speed air jet have a radius smaller than the target could cause an elastic deformation of the target surface, which has the potential to locally decrease the component of particle velocity normal to the surface.

As is visible in Figure 2.4, parts of the curved surface have a normal direction skewed at a large angle from the jet axis. Particles will be approaching the surface with a

slight angle to jet axis, due to flow effects in the deflection zone. As such, their impact on the surface would be at a non-normal angle, and with a lower component of velocity normal to the surface.

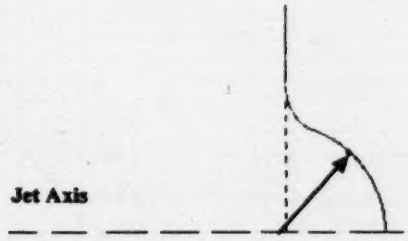

Figure 2.4: Schematic of a Vector Normal to the Deformed Target Surface

In addition, the flow streamlines would now change, and a particle would meet some resistance from flow with a component of velocity opposite to its motion, which would act to decelerate the particle. (As opposed to a flat surface, where flow components not in the same direction as the jet axis are radial outward, and as such should at most influence particle deposition location, rather than deposition speed.) Due to this decrease in normal velocity, and after the flow is removed from the surface, the surface would rebound to the position indicated by the dashed horizontal line in Figure 2.4, and the apparent penetration depth could be decreased. The total reduction in the normal component of particle velocity was numerically modeled by Hardy and Kendall (2005), and was found to be as high as 30%.

2.3 – Revised Prediction of Particle Penetration

Given the above theory, it seemed prudent to go back to the original penetration depth prediction made at the end of section 2.1, and revise the estimate to account for the effects on velocity that the jet would potentially have. All parameters save for velocity were kept identical, and the velocity was then scaled. It was assumed that the figure of 75 m/s was the exit velocity of the jet. Thus, to take a worst-case scenario, the impact velocity was reduced by 50% to account for the possibility of aerodynamic effects slowing the particles, and then reduced a further 30% to account for a curved surface lowering the local normal components of particle velocity. The results are shown in Figure 2.5 below.

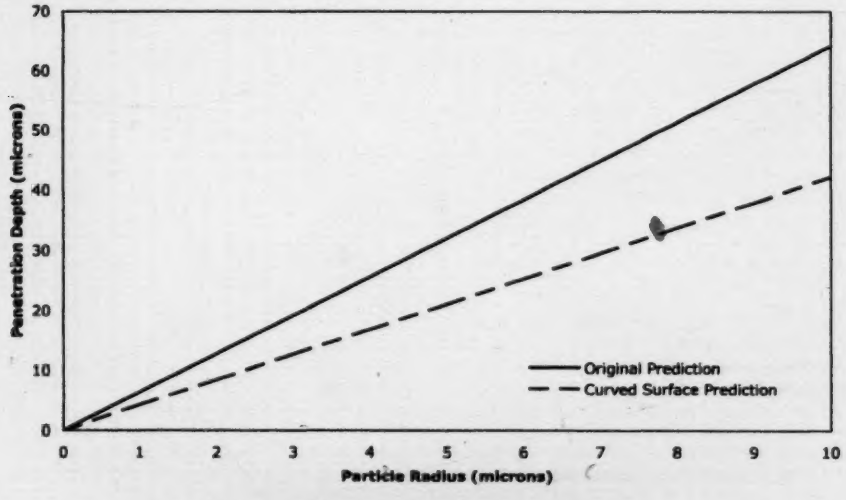

Figure 2.5: A comparison of predicted penetration before and after aerodynamic effects are taken into account

Despite the significant reduction in the particle velocity at impact, the predicted penetration depth for the largest (10 micron) particles was decreased by roughly 20 microns. Therefore it appeared as though there was still a significant opportunity for utilizing ballistic impact as a method for size-selective sampling of aerosol particles.

Chapter 3

Experimental Design

In the course of theoretical work one design aspect was decided upon, namely that particles would be delivered to the target in a stream of high-speed air. This was only an added constraint to the design. To review the constraints outlined in Chapter 1, the final design needed to be robust enough to withstand in-situ conditions, be capable of remote operation, low cost, low weight, small in size, consume as little power as possible, and provide an unbiased sample of particle size distribution. However, as this is a proof of concept, it was decided to focus on finding a material suitable for ballistic sampling of aerosols, and leave overall instrument design for future work.

3.1 – Target and Particle Material Selection

There were two main material decisions to be made: most importantly, the impact medium to be studied, and secondly, the particles that would be fired into the impact medium.

3.1.1 – Impact Medium

A range of materials were considered early on for their utility as a medium that would allow ballistic behavior at low energies. Porous media were identified quickly as

being the most likely candidates to fulfill this need, though they would need to be easily made with a uniform porosity, so that they would provide repeatable results for particle penetration.

Gelatin is commonly used in high concentrations (typically 10 to 20 percent by weight) for ballistic testing on the much higher energy scales of bullet penetration studies. It is a cheap, easily to acquire material that generally provides uniform porosity. As well, during the preparation of gelatin specimens, adding a fluorescent dye (or some other method of tagging the gelatin) is a trivial task. Additionally, its strength is highly dependent on the concentration of the gelatin, (Groot, et al., 1996) which means a low concentration gelatin may allow for ballistic behavior on a small scale as well.

Gelatin's primary drawback as a material for ballistic impact is that its strength is also temperature dependent. As its temperature increases, its strength decreases up until the point it finally melts (typically 35 °C). However, if the temperature were controlled, this would not pose a problem to the experiment. The freezing temperature of water also limits gelatin as an impact medium. It was observed that when frozen, the water dissociates from the gelatin and forms small ice crystals, changing the microstructure and characteristics of the gelatin entirely. The temperature of most commercial refrigerators (usually 4 °C) would possibly therefore be an ideal specimen temperature.

Thus, considering the above information, it was decided to investigate the utility of low concentration gelatin as a medium for ballistic impact of aerosol sized particles. Knox brand gelatin was purchased for this purpose. While there exists some data for the yield strength of gelatin at low concentration (Groot et al., 1996) the author is not aware

of any that deal specifically with this gelatin. As such, tensile tests of the gelatin would be required to obtain this data.

3.1.2 – Particle Material

In order to more easily obtain a correlation between average depth of penetration and particle size, it was important that any particles used in the experiment be available in a highly monodisperse form. This way, the particles should penetrate to a relatively uniform depth 'band' which could be easily averaged. Additionally, it was preferable that the particles come in a dry powder form, for ease of ensuring particle size, as particles in liquid suspension may not lose all their surface water in flight to the target.

To more easily find penetration depth, it was also desirable that any particles used be able to be doped with a fluorescing dye, which could be easily picked up by a visual instrument, if one were used.

A company in Germany, Microparticles GmbH, was found to offer highly monodisperse particles in the size range of interest (less than 10 microns) with a coefficient of variation of less than three percent, and highly uniform spherical shapes.

This company offered particles made of Melamine-Formaldehyde (MF) Resin Particles, which could be doped with fluorochromes for particle fluorescence. MF Resin (chemical formula $(C_3H_8N_6O)_n$) has a density of 1.51 kg/m^3 and a refractive index of 1.68. Particles made from MF resin have a hydrophilic surface, and superior mechanical strength, which would prevent them from breaking up on impact.

It was decided to buy MF resin particles in three sizes: 10.60 ± 0.12 microns, 7.09 ± 0.16 microns, and 3.16 ± 0.08 microns. These particles would be doped with a dye

known as Fluorescein isothiocyanate (FITC). This fluorochrome (chemical formula $C_{21}H_{11}NO_5S$) has an excitation wavelength of 488 nm and has a fluorescence emission maximum at approximately 520 nm. (Microparticles GmbH website)

3.2 - A Tensile Specimen for Measuring Gelatin Strength

In order to measure the tensile strength of the 2.5% concentration gelatin, an iterative design method was employed to find a specimen that could support its own weight, such that it could then be properly loaded to its breaking point, and have the total load measured. One of the principal problems encountered was that of how to attach the gelatin specimens to any tensile testing equipment. After some testing, it was concluded that the best way to overcome this obstacle was to rely upon an interfacial bond between cast gelatin and an ABS surface. It had been observed during the testing procedures that this bond often appeared stronger than that of internal bonding of the gelatin. To this end, the specimen casting apparatus shown in Figure 3.1 was constructed.

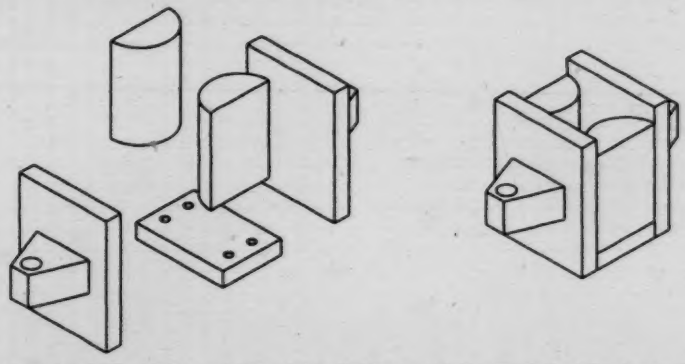

Figure 3.1: Regular, and 'Exploded' Views of the Tensile Specimen Mould

The two end plates were rapid-prototyped out of ABS, and featured protrusions for coupling the specimen to an apparatus for applying a tensile force. The other pieces were machined out of aluminum. In planes parallel to the end plates, the cast specimen

would have a rectangular cross section. Perpendicular to the plates, the specimen would taper towards the center of the specimen in a semi-circular manner, as shown in Figure 3.2. The specimen would have a total length of 1.5 inches (38.1 mm), and a maximum width of 1.5 inches (38.1 mm) as well.

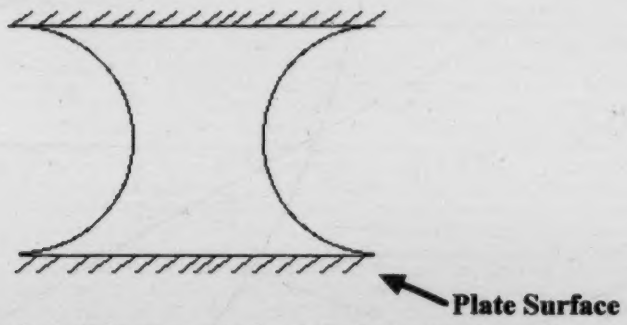

Figure 3.2: Cross Section of Gelatin Tensile Specimen Perpendicular to Plate Surfaces

The semi-circular mould pieces had a radius of 0.5 inches (12.7 mm), thus giving the tensile specimen a width of 12.7 mm at its narrowest point.

Prior to specimen casting, the aluminum pieces were coated with high vacuum grease in order facilitate ease of removal before tensile tests were undertaken. During the removal, the aluminum pieces were also warmed under a stream of water to further aid in removing them from the gelatin specimen without physically damaging the specimen.

3.3 – Modeling Extreme Conditions

Since the final goal of this study is to have a complete remote aerosol sampling package for difficult to reach environments, thought was given to what conditions to attempt to test within. The most extreme environmental case considered was that of the Martian surface, which has an atmospheric pressure which is only 0.6% of Earth's, and whose mean surface temperature is -60 °C. (Mars General Circulation Modeling Group at

NASA Ames, 2004) There were no facilities available that could provide this temperature for experimentation, and given that the Martian surface can reach temperatures as high as 20 °C, it was decided that experiments could be carried out at room temperature, with the target samples refrigerated at a temperature of approximately 4 °C. Experimentation within this temperature range was considered to be reasonable, given the conditions above.

To model the pressure difference, a clear cylindrical vacuum chamber was purchased from LACO Technologies (www.lacotech.com), and equipment procured as illustrated in Figure 3.3. The chamber had an internal diameter of 7.5 inches (19.05 cm) and a height of 12 inches (30.48 cm). The chamber lid was held on and sealed by lining the top of the cylinder with a rubber gasket, and then relying on the ambient pressure to hold the lid in place as the chamber was evacuated. It was found that the chamber could be evacuated to a vacuum pressure of -28.5 inHg (-96.5 kPa), or approximately 4.7% atmospheric pressure. The particles would be fired from the side, driven by atmospheric air rushing into the evacuated chamber (after snapping open the ball valve), into a gelatin specimen held such that the air jet would be perpendicular to the gel surface.

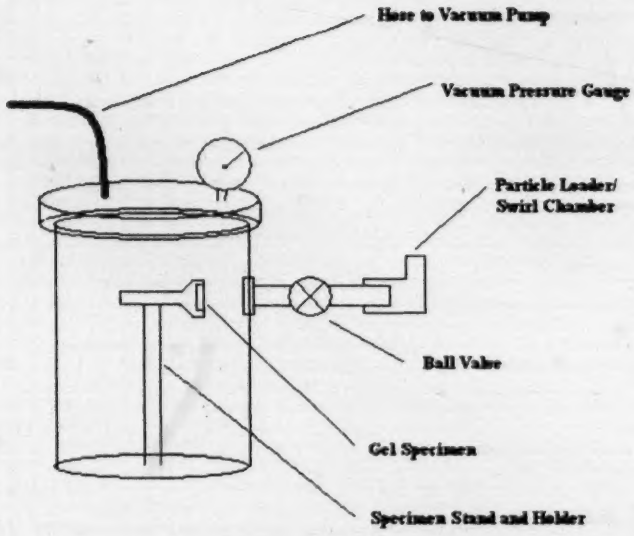

Figure 3.3: Vacuum Chamber Apparatus

Primary tests seemed to indicate this would allow for particle penetration, however it was discovered that the geometry of the cylinder made measurement of particle speed quite difficult, and there was no systems available and functioning which could measure within the chamber volume. It was therefore decided to move to an atmospheric apparatus, where the test could be operated in open air. While the simulation of Martian atmospheric pressures was lost, it was believed that there should be no significant change in the physics of particle motion, provided the particle-laden air jets were of the same speed. The primary difference would be that the jet would not expand nearly as much in atmosphere, as it would in the vacuum.

3.4 – Measuring Particle Speed

There were two main methods that could have been used to measure the particles' speeds: Particle Image Velocimetry, and Laser Doppler Anemometry. However, prior to

choosing which method to make use of, it was first necessary to estimate the rough speed of the air stream in the vacuum chamber, so that the appropriate system could be chosen which could measure within the required speed range.

3.4.1 – Estimation of Particle Velocity in Vacuum Chamber

It was at first mistakenly assumed that the air jet in the vacuum chamber would be sonic for the duration of the particles' flight. It was realized though, that this would not be the case. Rather, since the opening the air first entered the apparatus was 0.3 inches (7.62 mm), then expanded into a 0.75 inches (19.05 mm) main horizontal pipe, that the air jet itself would be significantly slower than sonic.

A highly simplified analysis was made on the average speed of the air stream in the 19.*05* mm pipe while the pressure difference between atmosphere and the inside of the chamber was high enough to keep the flow choked at the 7.62 mm inlet. Taking the average speed at the inlet as 343 m/s (the speed of sound at standard temperature and pressure), it was possible to find a mass flow rate of air into the inlet, while this velocity was constant. Since this mass flow rate of air must be the same within the 19.05 mm pipe, it was possible to calculate an average velocity of approximately 55 m/s.

The only other consideration to take into account was whether the particles would reach the target before the backpressure increased to a high enough level to slow the air at the inlet to subsonic speeds. It was calculated that the longest distance the particles in the vacuum chamber would need to travel would be approximately 35.5 cm, which at 55 m/s would take the particles roughly 6.5 ms. It was calculated that it would take the vacuum chamber 0.38 s to reach a high enough back pressure to slow the inlet flow to below

sonic, and so 55 m/s seemed to be a reasonable estimate of particle speed. Thus, any atmospheric pressure apparatus would need to be able to accelerate the particles to this speed or higher, and any device used to measure particle speed would need to be able to measure these speeds, for particles as small as 3 microns.

3.4.2 – Particle Image Velocimetry

Particle Image Velocimetry (PIV) relies upon high quality optics and a laser light source optically formed into a sheet of light. This sheet of light will illuminate small particles following the direction of flow, and when the light is strobed at a high rate (typically in the range of several milliseconds) two consecutive images can be broken up into "interrogation volumes" with an image processing program, which can be processed and interpreted in order to extract the characteristics of the flow being examined.

PIV is advantageous in that it can extract velocity information for a relatively large field of flow, provided that the light sheet can be properly positioned. Because it relies on a single sheet of light, and a camera perpendicular to the light sheet, it can also take velocity information right at the surface of any object immersed in the flow.

However, PIV has several limitations, mostly due to the limitations of hardware used. This includes the need for a relatively dense particle field in order to take accurate correlations from images, and the time cameras would need between exposures, as well as time the laser would need to recharge between light pulses.

These, combined with the limited ability of the camera and/or computer images in real time, would at the very least require a triggering system to be put in place prior to taking measurements.

These limitations, combined with the lack of availability of a function PIV system, disqualified using PIV as a viable option for measuring particle speeds.

3.4.3 – Laser Doppler Anemometry

Laser Doppler Anemometry (LDA) relies upon light interference patterns and the Doppler shift in order to measure particle velocity within a small "probe volume" formed by the intersection of two beams of laser light.

Typically, a Bragg cell splits a single continuous pulse laser beam into two beams, one of which has its frequency phase-shifted by a known increment. These two beams are fed into a probe, where a lens focuses them onto a common intersection point that creates the probe volume, as shown in Figure 3.4.

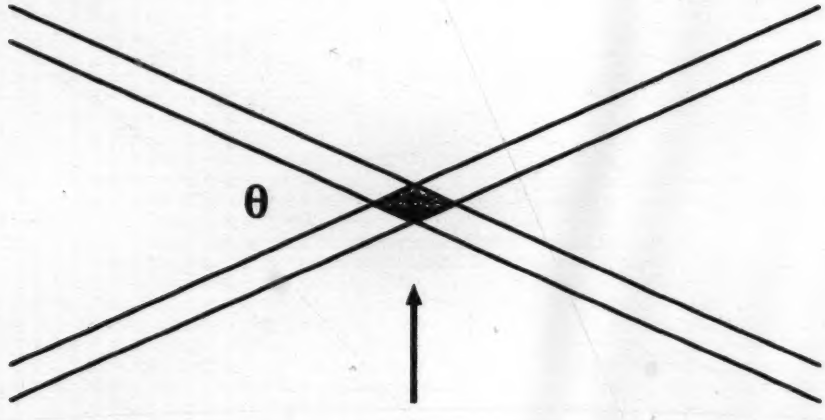

Figure 3.4: Top View of the Probe Volume, With an Arrow Showing Direction of Particle Motion

Light interference due to the intersection of beams of two different phases results in parallel regions of high light intensity, known as fringes. These fringes have a spacing determined by the laser wavelength, and the angle of beam intersection. As a particle

passes through the measurement volume, it scatters light proportionally to the intensity of the light in the region it is passing through.

This scattered light is then picked up by a photo detector and is converted into an electrical signal, the Doppler burst, which is sinusoidal with a Gaussian profile due to the intensity of the laser beams. A Doppler frequency can be found from this signal, the inverse of which is the time it takes the particle to travel between two fringes. Thus, with a known fringe spacing and Doppler frequency, particle velocity can be easily determined.

The main drawback to this method of velocity measurement is that it only measures velocity in a single location at any given time, so the amount particles decelerate as they approach the target remains unknown. As well, due to the intersecting beams, there is a fixed closest distance to the surface that the probe can be positioned to. Any closer, and one of the two beams would be disrupted, thus making it impossible to make a measurement.

This system of measurement can take instantaneous velocity measurements in one dimension for each set of intersecting beams of light. It also can automatically average multiple velocity readings into a single average, whose accuracy and root-mean-square (RMS) deviation will increase in accuracy with increasing sample number. Therefore, much like the PIV system, it is desirable to have as large a number of particles pass through the measurement volume as possible.

Based on the required velocity measurement range and other considerations above, it was decided to make use of a Dantec LDA system in the Aerosol Research Laboratory of Alberta. This system makes use of a 632.8 nm HeNe laser, split into

beams with a Gaussian diameter of 0.68 mm, and a beam intersection angle of 13.61 °. Its fringe spacing is 2.67 microns and has a maximum velocity measurement range of -16 m/s to 80.09 m/s.

3.5 – Measuring Particle Penetration Depth

With a method for measuring particle velocity decided upon, the next problem to be solved was the question of how to measure depth of penetration of the particles fired into the target. The problem had two main parameters: the location of the target surface must be found, and then the distance from that surface the particles traveled had to be measured.

Physically sectioning the target after firing would have definitely allowed for easy measurement of both these parameters, but as the end goal was to eventually develop a remote system, it was decided to pursue non-destructive means of measuring the depth of particle penetration which could possibly be remotely operated.

3.5.1 – X-Ray Imaging

X-Ray imaging was the first alternative considered for determining particle depth. There exist today high-resolution digital x-ray imaging systems that can fit onto a bench-top, such as those manufactured by Micro Photonics (www.microphotonics.com).

Such imaging systems are advantageous in that they can image small-scale structures in any material that is permeable to x-ray radiation. Thus, the target material need not be transparent for this method of measuring penetration depth to be effective.

The resolution of x-ray imaging is controlled primarily by the quality of the camera used; the resolution must be only a few microns per pixel in order to accurately interpolate the location of micron-sized particles. (microphotonics.com/skymto.html)

The major drawbacks to the use of such an instrument would be that in an in-situ situation, a sensitive piece of equipment such as this could be prone to failure, and generally has a high power requirement. Additionally, there existed no equipment of this resolution available for use in experimentation, so this option was not examined further.

3.5.2 – Confocal Microscopy

A confocal microscope uses laser-excited fluorescence to accurately locate feature depth in the traditionally two-dimensional field of view common to most microscopes.

In confocal microscopy, a focused beam of laser light is reflected off a "dichroic" mirror (that is, a mirror that will reflect light of certain wavelengths, but allow other wavelengths to pass through) and through the microscope objective lenses onto the object being examined. If this object is doped with a fluorescing dye, the laser light will cause the area of the specimen it hits to emit light of a certain wavelength.

The light emitted by the fluorescing specimen area travels back up the objective lens, and through the dichroic mirror where it can be detected by a camera, or the human eye. (While the laser light itself is filtered by the mirror)

In a typical microscope, there is no way to filter out light coming from outside the focal plane of the lens system. However, if a plate with a "pinhole" is put between the lenses and whatever method of light detection is being used, this problem can be mitigated, as is illustrated in Figure 3.5.

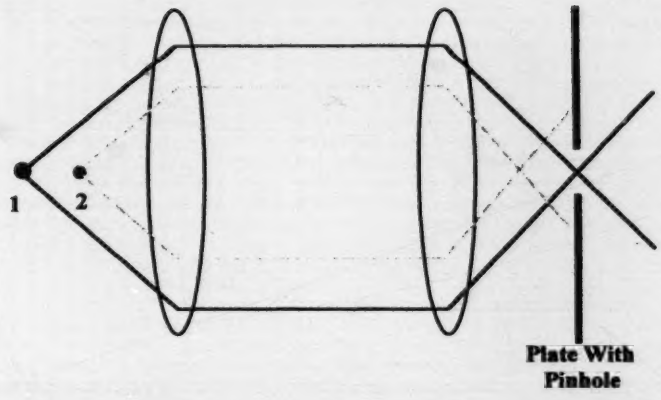

Figure 3.5: Illustration of Pinhole Filtering Out-of-Plane Light

Point 1 in the figure above is a fluorescing point within the focal plane of the lens system shown. The light from this point is allowed to pass freely through the pinhole and continue on to the detection system. On the other hand, because point 2 is out of the focal plane, most of its light is blocked by the plate, and not allowed through. The pinhole is said to be at the conjugate point to the focal point of the plane in which point 1 lies, which is where the "confocal" microscope gets its name.

By combining the pinhole and laser systems with a set of scanning mirrors, the laser can be scanned across a field of view, and the resulting fluorescence picked up by a computerized system can build an image of the fluorescing structures within the plane being viewed. If a micro-stepping motor is attached to the fine focus control of the microscope, the microscope can the "step" between consecutive focal planes, effectively optically sectioning the material through its depth.

This type of system is limited both by its power consumption, and by the necessity of a target medium that is transparent. Since gelatin was the material chosen for examination, this second limitation was not a problem for current experimentation, though in an in-situ measurement system, power consumption may be an issue.

Traditional optics of this sort may be sensitive to the vibrations encountered by a future system on its way to the area it is sent for aerosol collection, though it may be possible to design a system that could possibly survive such vibrations.

This system is advantageous in that such systems are already mostly automated, and provide excellent resolution in measurement of focal plane distance, and can even be used to build three-dimensional images of the specimen being scanned.

Use of a confocal microscope also opens up other avenues of possible analysis, were it to be used in a final design of an in-situ particle collector. Since the microscope could in theory be used to also size particles collected, this combined with the theoretical equation developed for ballistic penetration (equation 11) could technically make it possible to determine the density of the particles collected, which could aid in material identification, if the nature of the aerosol collected was unknown.

Given the above considerations, it was decided to pursue the use of confocal microscopy for measurement of the particle surface location, and depth of particle penetration. To locate the surface, it was decided to lace the gelatin with Acridine Orange, a fluorescing dye with peak excitation and emission wavelengths of 500 nm and 530 nm respectively. Since the particles selected are laced with FITC, the confocal microscope will be able to filter each dye's emitted light separately, to avoid interference between the detection of either surface location, or particle penetration depth.

The confocal microscope used was a Leica TCS-SP2 Confocal Laser Scanning Microscope, owned by the University of Alberta Biological Sciences Advanced Microscopy Unit. This microscope made use of two lasers: a 488 nm Argon-ion laser,

which would excite the FITC dye, and a 543 nm Helium-Neon laser, which would excite the Acridine Orange dye.

3.6 – Overall Apparatus

With the methods for measuring particle speed and penetration decided upon, all that remained was to put an entire experimental apparatus together.

3.6.1 – Gelatin Concentration and Target Specimen Shape

As the gelatin target specimens were to be placed under a confocal microscope, it was decided that the target specimens should be cast into glass-bottomed dishes, such that light could pass freely through the entire specimen. Such dishes were found to be available from Electron Microscopy Sciences (http://www.emsdiasum.com), with petri dish configurations shown in Figure 3.6 below.

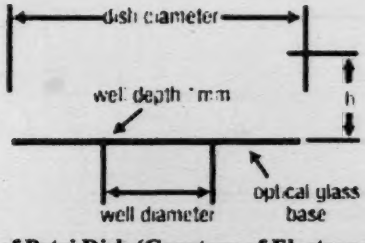

Figure 3.6: Cross Section View of Petri Dish (Courtesy of Electron Microscopy Sciences' Website)

The dishes purchased were 35 mm in diameter, 10 mm in height, and had a well diameter of 22 mm.

To further ensure that the gelatin had a flat surface, such that there would be no optical distortion due to a curved gelatin surface, it was decided that when specimens were cast, they would have a standard microscope slide placed across the top while the

gelatin was still in its unset, liquid phase. It was found this slide could be easily removed after casting, leaving behind a uniform, flat target surface.

In order to determine which concentration of gelatin to be used, specimens were cast at known concentrations into the specimen dishes. The gelatin was mixed according to the instructions on the Knox brand gelatin packaging, and then had 18-20 drops of 0.1% Acridine Orange solution mixed in.

Once cast, each specimen was subjected to a burst of air in the vacuum chamber apparatus, and then inspected for signs of tearing or other destruction of the gelatin target.

In order to maximize penetration, it was decided to find the lowest gelatin concentration possible that would withstand the burst of air without suffering permanent damage. This would make the gelatin tensile strength as low as possible, allowing for deepest penetration of all particles. Through an iterative process, this concentration was found to be 2.5% by weight.

3.6.2 – Particle Firing and Deaggregation

Two primary design considerations firing the particles were the issues of how to get the particles entrained into a positively pressurized air stream, and how to ensure any agglomerated particles were separated into their individual constituents prior to impact.

Entraining particles into a pressurized air stream is difficult, as any opening into a pressurized line will inevitably result in flow out of the line, and is problematic when the desired outcome is to place new material into the air running through line. After some consideration, it was decided that a 'slider' mechanism, containing several sections of pipe could be built, and made a part of the system's air line. Thus, while it would briefly

interrupt the air flowing through the line, it would be possible to place charges of particle powder directly into the air stream.

In order to hold the powder in place properly, the line would either need to be horizontal at this point and allow particle entrainment in the pipe wall boundary layer, or else have some form of simple "ledge" or other horizontal surface in the pipe from which the particles could be entrained into the air stream.

The solution arrived at for the case of a vertical pipe was to place a small plastic valve commonly found in condiment and sport drink bottles. This simple device is a plastic well with a 'cross' shape cut into the bottom, as shown in Figure 3.7.

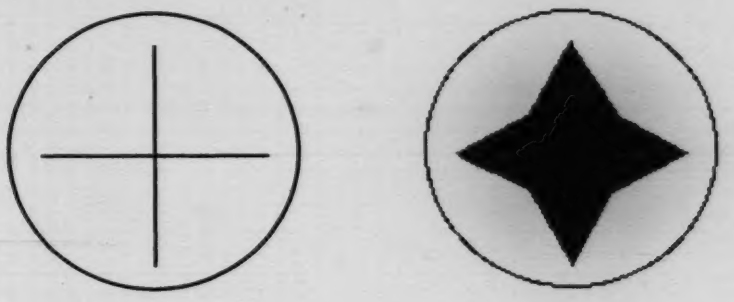

Figure 3.7: Top View of Plastic Valve when a) Closed, and b) Opened

When a pressure drop is applied across this well, the flaps created by the cross cut bend open, to allow anything behind the valve through. Therefore, such a valve could be placed into the vertical pipe, and would hold the particles in place until inserted into the pressurized air stream. This has the further advantage of placing the particles immediately into the air stream, rather than relying on aerodynamic forces in the boundary layer to entrain the particles.

In order to ensure the particles do not stick together as an agglomerate (due to electrostatic forces between them) it was also necessary to ensure some method of deaggregration was present in the particle firing system to separate any potential agglomerates into their constituent particles.

One such possible method was to introduce turbulence to the air stream. According to Finlay (2001), turbulent eddies on the integral scale of motion can provide adequate force to remove particles from agglomerates through rolling, sliding, and lifting of individual particles.

The question of how to introduce turbulence was of concern, but a solution to the problem was found. A dry powder inhaler developed by Wang et al. (2006) was found, which relies on forcing flow through a cyclone chamber to generate strong air circulation for effective deaggregation. It was decided that the geometry of this inhaler, adapted and scaled to the appropriate size, would be used to ensure particles arrive at the target as individual projectiles.

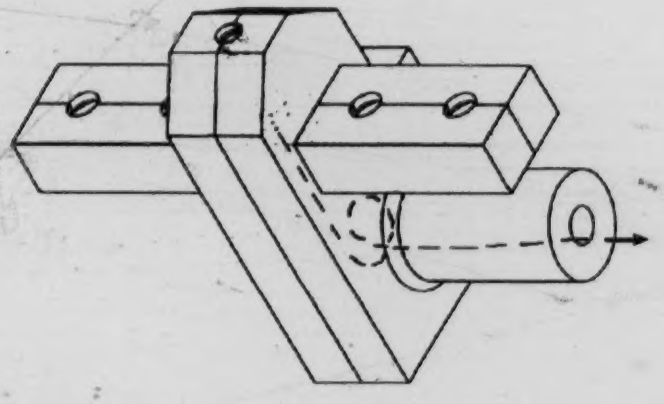

Figure 3.8: Particle Firing Assembly, Showing Internal Geometry

Figure 3.8 above shows the final design combining the cyclone chamber of Wang et al., and the slider mechanism discussed earlier in this section. The slider moves horizontally, allowing a plastic 'cross' valve holding particle powder to be placed into the vertical air stream, which would enter at the top of the device. The flow would continue downward into the cyclone chamber, and then exit horizontally, as illustrated by the black dotted line. To give some sense of scale, the entry hole at the top was designed to accommodate a Teflon hose with an outer diameter of 0.25 inches (6.35 mm), and the cyclone chamber was approximately 49 mm in diameter. The apparatus was made of acrylonitrile-butadiene-styrene (ABS) plastic using rapid-prototyping stereolithography. The internal surfaces were smoothed to prevent excessive particle deposition by applying methylene chloride to the surfaces.

It was found during apparatus testing that the large diameter exit hole was too close to the swirl chamber, such that the flow had insufficient time to straighten following exit the cyclone chamber. It was decided therefore to place a cone over the exit structure, which would constrain the flow horizontally for another 20 *cm*. (Figure 3.9)

Figure 3.9: Schematic of Cone Attached to Particle Firing Assembly

In addition, in order to minimize the size of powder charge needed to give sufficient particle density through the measurement probe of the LDA, this cone was tapered, such that the flow would exit with a jet diameter of 0.1875 inches (4.76 mm).

3.6.3 – Complete Apparatus

The complete apparatus was set up, such that particles could be fired manually in concert with activating the Dantec LDA for particle speed measurements.

It was calculated that when placed into a holding device, the closest the gelatin specimen could be to the LDA measurement volume was approximately 7 mm, or nearly 1.5 jet diameters. Thus, instead of measuring particle speed directly, it was decided to measure the particle speed approximately 1 jet diameter from the exit of the complete particle firing assembly. Total distance from the jet exit to the target was approximately 3 jet diameters. This set up is illustrated in Figure 3.10.

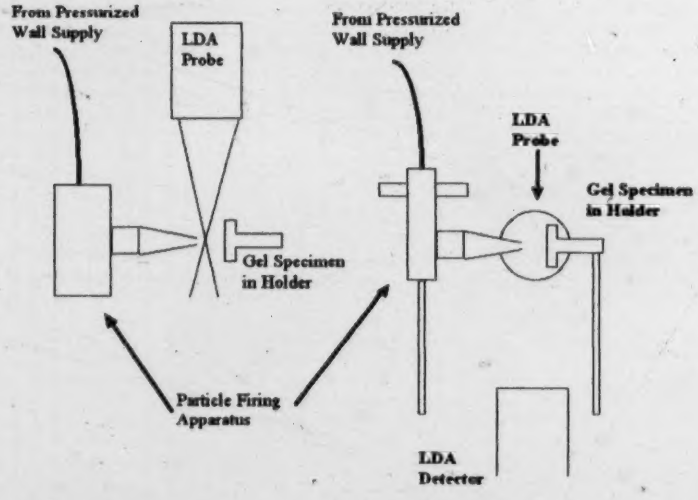

Figure 3.10: Schematic of Complete Particle Firing Apparatus. Left: Top View. Right: Front View

Given that particle impact speed could not be measured directly, it could be estimated based on the considerations examined in the theory section. At the very least, a correlation could be drawn between jet velocity, and particle penetration depth, which could still be a useful correlation for an in-situ particle-sampling device.

With this apparatus complete, a gelatin sample could have particles fired in to it, with particle speed measured, and then be taken to the microscopy lab for measurement of penetration depth.

Chapter 4

Results

4.1 – Gelatin Tensile Strength

Tensile specimens were attached to a weight placed on a scale, such that as the tensile specimen was lifted, it could be observed how much load it removed from the scale prior to breaking. As it was observed that under its own weight, the tensile specimen would stretch from its cast length, it was decided to weigh the lower half of the broken specimen, and add its weight to the total load the specimen lifted prior to breaking.

Specimens that did not break at their center were considered invalid results; however, their breaking strength was still estimated in order to give an idea of what strength a properly breaking specimen should exhibit.

After several trials, one specimen was ruptured along the center of the specimen, and its final load at rupture was found to correspond to a stress of 1.65 kPa. This value was found to be close to estimates made from improperly broken specimens, as well as similar gelatin measurements made by Groot et al. (1996). Therefore this value of tensile strength was assumed to be valid.

4.2 – Particle Penetration Depth Measurements

Particle penetration depth was measured using optical sectioning capabilities of confocal microscopy. The microscope control software allowed for optical sections of known size and depth to be taken. Typically, single sections were approximately 1 micron thick, and were spaced, center-to-center, a distance of 0.98 microns apart.

The first of many problems were recognized upon attempting to find the surface location by looking for the loss of fluorescence as the microscope focal plane moved outside the gelatin surface. Rather than finding a distinct boundary, it was discovered that the fluorescence from the Acridine Orange dissolved into the gelatin would slowly fade, over a distance of tens of microns. This meant that there was some "bleeding" of light from other focal planes into the current one. While this could be mitigated somewhat by averaging the image several times to filter out noise, no sharp boundary could be reliably found. Typically, captured images were averaged four times. It was further observed that the detection bandwidths for both the green and red fluorescence overlapped, especially into the more sensitive red fluorescence detection.

Figure 4.1 (below) illustrates some of these phenomena. While part a) of Figure 4.1 is showing the beginnings of loss of red fluorescence detection, especially near the corners, the middle still shows a great deal of fluorescence. Contrast this with the red fluorescence field of part b), which is roughly 29 microns deeper into the gelatin. As can be seen, finding the gelatin surface is problematic.

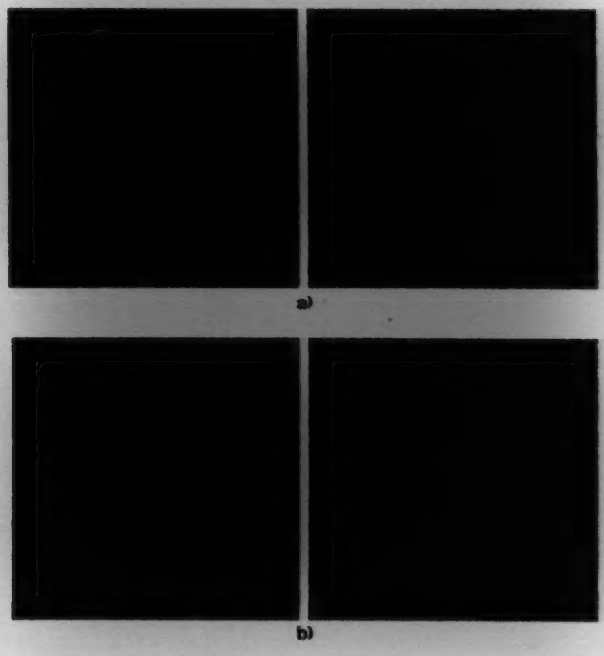

Figure 4.1: a) A sample of cross sections near the surface, and b) Near the bottom of the particle field. Green Fluorescence is shown on the left, Red on the right.

Different ways of doping the gelatin with Acridine Orange, such as placing it on the gel surface after casting specimens, were tested. However, these proved to exhibit the same fluorescence behavior under the confocal microscope.

Further examination also revealed that this "bleeding" of fluorescence into other planes was also occurring for the fluorescence emitted by the fired particles, such that they appeared in a series of sections far thicker than the diameter of the particle. Again, while image averaging would mitigate this problem somewhat, it would not do so entirely. Consulting with the head of the microscopy lab confirmed that this could sometimes be a problem, and that the solution was to find the point where the particle exhibited its largest diameter, and brightest fluorescence. Since any given section may not necessarily fall right on the centerline of a particle, this method would provide a way of finding the midplane location of the particle to within 1 or 2 microns.

Thus, in order to measure the penetration depth of particles, two related problems had to be overcome: finding the midplane of the particles, and finding a way to locate the target gelatin's surface. It was decided that rather than continue to dope the gelatin with Acridine Orange, the surface could instead be dusted with particles of a different size following the firing of the first particles. Specimens are examined "face down" on the microscope, resting on a microscope slide. It was therefore decided that the best manner in which to dust the surface following particle firing would be to dust the microscope slide upon which the target would rest. This would prevent particles from being given any velocity with which to penetrate the target themselves, and would further prevent the possibility of particles "sinking" into the gelatin due to gravity.

With the issue of finding the surface resolved, all that remained was to find a way to locate the optical section images in which the surface particles and the fired particles were each at their brightest, and widest diameters. To this end, an image processing program was written using MAT Lab, which would find and count particles in each section, then filter them according to their size and brightness. The final output would be a distribution of particles that are largest and brightest in each section image, which could then be averaged to find an effective midplane of both the gel surface, and the particle penetration depth. (A printout of this code can be found in Appendix A) Both sizes of particles (those on the surface, and those fired) would have a distribution outputted from a single run of the program.

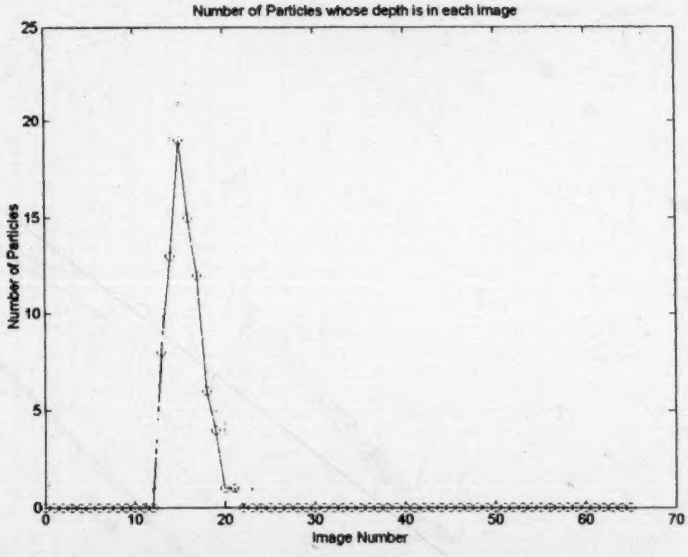

Figure 4.2: A plot of particle center location distribution for a series of gelatin section images

A fresh round of 10.6 micron particles were fired into the gelatin specimens, and the specimen surface was then dusted with 3.16 micron particles. As shown in Figure 4.2 above, an unexpected result was found: the particles on the surface (marked with a '+' sign), and the particles fired into the gel (marked with an 'o') appeared to be at the same depth! (Raw data can be found in Appendix B.) An averaging of number of particles per plane, and number of planes gave an average difference in depth of the particle midplanes of approximately 0.25 microns, which is far smaller than the measurement uncertainty of the microscope. Given the difference in mean particle diameters, and assuming that the smaller particles were just touching the gelatin surface, this would suggest a maximum penetration of only 4 μm.

The filtering values the program used to count particles based on diameter and average brightness were changed in order to see if this was a matter of the filtering improperly cutting out particles of the desired sizes. Since the MAT Lab functions

utilized in the program consider particle image area in pixels, it was thought that perhaps the conversions calculated initially might have been incorrect. However, regardless of the sensitivity that the filters were set to, the result remained the same: the image processing program output suggested that the particles did not seem to be penetrating the gelatin.

To check this result, one final specimen was prepared, and 10.6 micron particles were fired at the specimen once more. This specimen was then physically sectioned, such that the view would not need to be optically sectioned; rather, the gelatin target specimen could be viewed from the 'side,' relative to the direction of particle impact. A schematic of how the specimen was viewed is shown, along with images from the investigation, below.

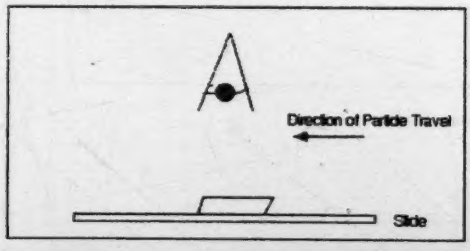

a)

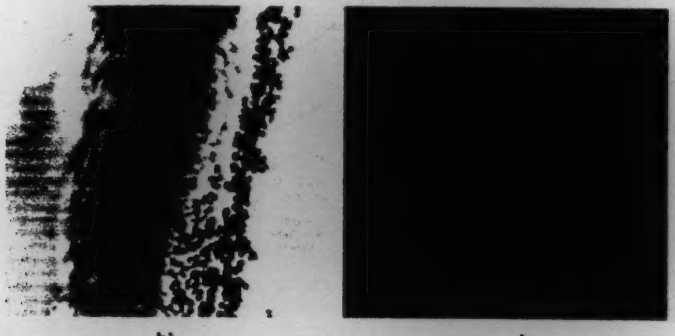

b) c)

Figure 4.3: a) Schematic of how the Specimen was viewed, b) Transmission image of the section, c) Fluorescing Image from a plane within the specimen.

As can be seen, the particles are almost entirely resting on, or just inside, the surface of the gelatin. The fluorescing image in part c) of Figure 4.3, taken deeper within the specimen, confirms this result. The transmission image shows clearly that throughout the depth of the gelatin section, the particles fired are resting at, or perhaps just below, the surface.

4.3 – Particle Velocity Measurements

Particles were fired into gelatin targets using the positive pressure particle firing apparatus, supplied with a compressed air line regulated to a line pressure of 50 psi (344.7 kPa). This pressure was settled upon through iteratively testing the system until a pressure was reached that was in the upper end of the Dantec LDA's velocity measurement range, without going above the maximum measurable velocity.

This firing condition led to an average particle velocity of 68.2 m/s with an average RMS error of 5.89 m/s for the 10.60 micron particles. The Standard Deviation of these values was 3.34 m/s and 2.48 m/s respectively. The LDA made an average of 153 attempted samples per firing, with an average validation rate of 69%.

Due to the fact that particles were not showing ballistic behavior, as was found in section 4.2, no further velocity measurements were carried out.

Chapter 5

Discussion

There are many parameters to consider when examining the negative results of the experiment. It is important to consider if and why the particles fired into the gelatin did not actually exhibit ballistic behavior, so that future examinations of suitability of other materials for use in particle collection and sizing may benefit from the lessons learned from this experiment.

5.1 – Measurement Accuracy

In all experiments, it is important to consider how accurate the measurements taken were. As there will always be uncertainty, quantification of this uncertainty will help to explain deviations of the experimental data from the behavior predicted by theory.

5.1.1 – Gelatin Tensile Strength

The measurements of gelatin tensile strength had several sources of uncertainty, whose effects may be difficult to fully quantify. These sources included: uncertainty introduced by the method of measurement, uncertainty due to lack of measurement repetition, and uncertainty produced by complications during removal of the gelatin specimen from its mould.

As was previously stated, the measurement of tensile force prior to breaking was not made using a tensile testing machine, but instead was made by lifting a known weight

resting on a scale, and observing the total weight lifted off prior to the gelatin breaking. Since the breaking was a relatively quick event (i.e. less than a second in duration) the best resolution to which the measurement of lifted mass could be said to be no better than 0.1 grams.

To find the effect this would have had on calculated tensile strength, the accuracy of the specimen dimensions must also be considered. Skilled machinists can typically produce a part to within $\pm$ 0.015 inches (0.381 mm), and often to an even narrower tolerance. Taking this outside tolerance for the construction of the mould, along with assuming gravity as a constant g = 9.81 m/s, the error in the measured tensile strength is:

$$\Delta\sigma_T = \left|\frac{g}{lw}\right|\delta m + \left|\frac{-mg}{l^2 w}\right|\delta l + \left|\frac{-mg}{lw^2}\right|\delta w = 2.1Pa. \qquad (14)$$

This value itself is relatively small compared to the measured level of strength. There was, however, one further source of error due to the method of measurement. Since the specimens were not pulled apart using a tensile testing machine, there is no guarantee that the forces applied to the specimen were perfectly axial. While every effort was made to ensure the force was applied straight along one axis, there still could have been improper alignment during specimen loading. This possible lack of uniaxial force application could have led to stress concentrations building up locally at one location within the specimen. Such a concentration would inevitably lead to rupture a lighter load than the specimen ought to bear before breaking, and therefore a smaller load than the specimen was capable of bearing could have been recorded.

A simple angle calculation showed that for the axial force applied to a specimen to be reduced by 5%, the specimen would have to be held at an angle of 18.2 degrees off the loading axis, in any single direction. During testing, the angle the specimen was

pulled at was small enough to be below the resolution of the eye, and therefore was likely less than 20 degrees. The author is thus of the opinion that the error introduced by this phenomenon is as high as 10%, or 150 kPa, in the worst-case scenario.

Certainly, this error would have been mitigated by successful repetition of the tensile testing. However, with successful results coming only once out of every ten attempts (breaking at the center plane), time constraints made repetition difficult to achieve.

The final source of uncertainty in gelatin tensile strength measurements is from the method by which the gel was cast, and removed from its mould. As has been previously noted, high vacuum grease was applied to the aluminum mould surfaces in order to reduce bonding to the gelatin. This would result in small patterns imprinted into the surface of the gelatin. Due to the highly elastic nature of the gelatin, these may have had no effect, though it is possible that they could provide a small "stress raiser" on the surface of the gelatin.

The other uncertainty introduced by the procedure for removing a specimen from the mould is the need to slightly warm the aluminum surfaces to ease its removal without breaking or tearing pieces from the gelatin. Aluminum has a very high level of thermal conductivity, and thus warms quickly. It was observed that the gelatin surface would warm as well, though the core of the specimen, examined upon breaking of the specimen, remained cool. Due to the temperature dependence of gelatin, this would imply that the surface of the gelatin is somewhat weaker than the core. However, for the case of axial (or nearly axial) loading, it is possible that the effects of this warmer specimen surface can be neglected.

5.1.2 – Velocity Measurements

Due to the physics behind the operation of a Laser Doppler Anemometer, the instantaneous measurements of velocity require no calibration; fringe spacing and light scattering are known physical properties, and are essentially constant.

While instantaneous velocity measurements can be taken as accurate, it is the average velocity taken that is of concern. Typically, in a turbulent application, thousands of samples are taken at any one location in order to obtain a mean velocity. However, due to the highly transient nature of the experiment, such high sample numbers were not feasible. Fortunately, the data collected shows that despite the relatively low validated sample count, the mean velocity can be assumed to be accurate.

Table 5.1: Average Values of Data From Laser Doppler Anemometer

Avg. V_{mean} (m/s)	68.19
Avg. ΔV_{RMS} (m/s)	5.89
Avg. # Valid Samples	105.28

As is shown in Table 5.1 above, the RMS variance in velocity measurements was 5.89 m/s on average, which is 8.6% of the average mean velocity. The RMS values ranged from 2.75 m/s to 9.89 m/s, while mean velocities ranged from 64.76 m/s to 72.64 m/s. The largest RMS variances were, as expected, recorded for the lowest numbers of valid samples.

Given the above data, it would seem appropriate to assume that the velocities measured were, in general, correct to within 8-10%. Given that these measurements were taken approximately one jet diameter from the jet outlet, and impact speed was to be estimated from theory, this error would propagate through such calculations into the final predicted penetration depth for the measured conditions.

5.1.3 – Particle Penetration Depth

The uncertainty in particle penetration depth is primarily a result of uncertainties in the positioning readouts from the Confocal Microscope. The particle image-processing program used to locate particle midplanes within section images, as mentioned in Chapter 4, appeared to give penetration depth locations independently of the sensitivities of the image filters. While the program would detect more or fewer particles depending on the filter settings, the penetration depth profiles remained virtually identical.

Measurement uncertainty in the microscope is primarily due to physical limitations of internal stepper motors, and the optics contained within the microscope. Focal planes from which the confocal microscope would take fluorescent images were typically 1 micron thick, at most. Thus, any particle found to have its midplane within that image would actually be within ± 0.5 microns of that focal plane's location.

The confocal microscope software would typically give location readings to within 0.01 microns. However, it would also typically give the spacing between consecutive planes to 0.0001 microns. This latter accuracy is considered suspect in light of the former, and was ignored for the purposes of accuracy calculations. It seemed prudent overall, to assume the error in measurement was somewhat higher, and was taken for the purposes of calculation as 0.1 microns.

A particle's position would therefore be accurate to the sum of the errors due to both the focal plane thickness, and uncertainty as to its location, and would have a value of 0.6 microns. Since the surface location is also fixed by particle positions, it was assumed that a calculation of penetration depth by subtracting the two position values

would have an error of 1.2 microns (the sum of the errors of each location), or nearly 5 times the actual penetration depths measured.

5.2 – Examination of Results

It was found in Chapter 4 that the particles fired at the gelatin target deposited on, or just inside, the surface of the gelatin. This implied that either ballistic behavior was not present, or was at best, extremely weak for these aerosol particles. It was therefore important to examine the results in more depth, and attempt to determine what exactly was physically happening to the particles during the experiment.

To begin, the fluorescing image captured from the physical cross-section that was used to confirm the findings of the non-destructive test may be examined, and is presented in a larger size in Figure 5.1 below.

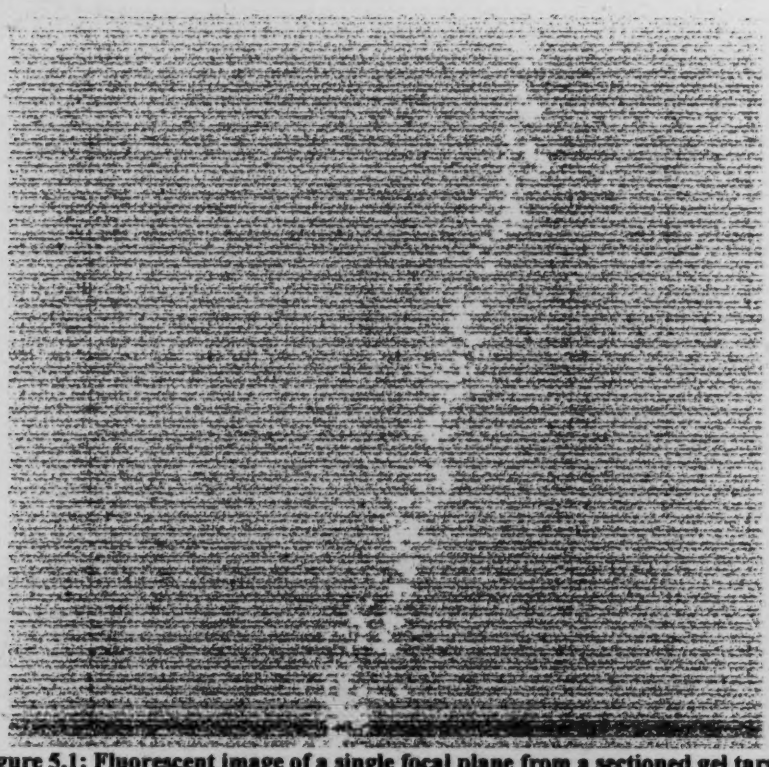

Figure 5.1: Fluorescent image of a single focal plane from a sectioned gel target

For reference purposes, the image shown in Figure 5.1 is 750 microns on a side, and is a capture of the fluorescence emitted from a focal plane roughly 1 micron thick, located somewhere inside the gelatin cross-section specimen. It has been converted to a black and white image to aid in examination.

To begin with, what the image is showing must be understood, so that it can be properly analyzed. First, what is noise, and what is not needs to be discerned. Obviously, the non-discrete 'glow' is noise produced by particles out of the focal plane. There is also some discrete noise present in the image: In the top, right-hand quadrant of this image, there are a few dimly illuminated particles to the right of the "main line" of particles. These particles are somewhat brighter than the noise surrounding them; however, they quickly 'blur' into this noise, and overall appear smaller than the particles in the main line. This would indicate that these particles' midplanes are residing just outside the focal plane, and one end of each of these particles is protruding into this focal plane. Thus, the only region of interest is the well-defined fluorescent particles running in the diagonal "main line" beginning at the bottom center of the image.

The first thing that is of note, is that the particles all seem to be clumped together within a region that is, at most, three particle diameters thick (approximately 31.8 microns). However, it is unclear from this image if they are resting inside the surface, or are being held in place on the surface by electrostatic attraction between particles.

It is further worth noting that the location of the particles infers that the surface is not perfectly flat. This makes sense given that the longer gelatin sits without a moisture barrier covering it, the more entrained water will evaporate into the surrounding air. Typically, it was observed that gelatin samples needed to age for 18-24 hours before the

specimen surface had a curvature visible to the naked eye. While this gelatin sample is at most two hours old and has been exposed to ambient air for 30 minutes at the outside, such evaporation effects would likely be first seen on a microscopic level as minor curvatures in the surface.

Furthermore, the distribution of the particles in this line may be indicative that if the particles have indeed penetrated into the gelatin surface, there may be open "voids" left in the surface behind particles. This could be a physical hole left in the surface at the point of particle impact which trailing particles could enter.

If the fired particles did penetrate the surface, the unusual shape of the surface and the corresponding distribution of particles may explain why smaller particles dusted on the surface gave a nearly identical location depth wise in confocal microscope section images. Specifically, open spaces behind a particle were originally assumed to close behind the particle, due to the highly elastic nature of gelatin. If this were not the case, particles dusted onto the surface could easily move into these open spaces, giving the result seen from the image-processing program. On the other hand, if the particles did not penetrate the surface, there would likely be enough open space remaining on the surface for these smaller particles to fill into.

Regardless, while this image sheds no further light as to whether the particles are on, or just below the surface, it can be said with some certainty that the tight grouping of particles seen in the image-processing program outputs is, in fact, correct.

In order to determine the location of the particles relative to the gelatin surface, the light transmission image was examined, and is shown in Figure 5.2 below. This image is of an area 750 microns square, and is in focus at the same plane as the image in

Figure 5.1. However, due to the nature of this image, all out of plane objects are also visible, though they are out of focus.

Figure 5.2: Transmission Microscope Image of the Sectioned Gel Target

Care must be taken when examining this image, due to the immense amount of out-of-focus particles visible. Recall that in Figure 5.1, the particles lying in the focal plane were in a line, starting at the bottom center of the image, and sloping upwards to the right. These particles are still visible, as shown by a series of light "dots" indicating where in-focus light is passing through these melamine resin particles. To the right of these particles is the foreground; to the left is the background.

It is also immediately noticeable that the extreme left and right ends of the image are of different shades. This is indicative of the consistently darker gelatin to the left, and the much lighter open air (and bare microscope slide) to the right.

A preliminary examination reveals, that as was now expected, almost all the particles appear to be resting in a narrow band on, or just embedded into, the surface of the gelatin. But there are five particles in roughly the middle left of the picture that have definitely penetrated deep into the gelatin.

There are two possible explanations for the unusual behavior of these few particles. The first is that the blade used to cut the section from the specimen may have moved them, perhaps pushing them with the blade edge, or perhaps due to friction between the particles and the blade. The alternative explanation is that these few particles were at the leading "edge" of the air jet as it first exited the nozzle, and as such were not subject to the deceleration effects of surface curvature.

It is difficult to say which of these possibilities is more likely to be true. Scaling the simple measurement of the particle image relative to the size of the image would suggest most of these deeper particles are in the foreground, as they appear to be twice the size they ought to be, owing to their being out of focus. This means the particles could very well be sitting on the outside surface of the section, and were moved to their position by the action of sectioning the gelatin target to make this sample.

An examination of the majority of the particle field into and out of the plane of focus seems to show that like Figure 5.1 showed, the particles all lay within a narrow band. There is a clue as to the location of this band of particles relative to the surface shown in Figure 5.2, and that is the extremely bright areas in close vicinity to the particles.

This brightness is likely due to light reflection and refraction at the air-gel surface interface. Much of this surface is out of the field of view due to the angle of the surface

relative to the viewing direction, but the parts which are visible, due in part to breaks in deposited particles, allow for some investigation of the particle location. While these bright areas are not entirely in focus in all areas of the image, it is likely that what is true at these few locations the surface is clearly visible is true for the entire section's surface.

From examining these areas, some particles seem to be at least partially embedded into the gelatin, and others appear to be resting on the surface, or on other particles partly embedded into the surface. Based on this, a range of estimated particle positions is shown in the schematic Figure 5.3 below.

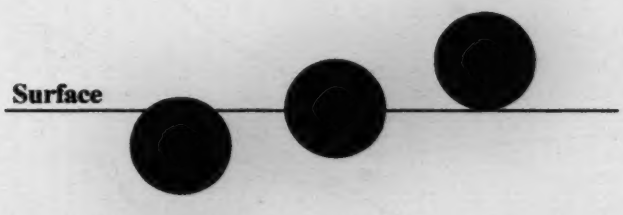

Figure 5.3: Schematic of estimated particle depth positions

As is shown by the representation of the particle on the left, it is thought that any particle that penetrates the surface does so minimally, and likely doesn't reach a mid-particle depth greater than a few microns. Particles seem most likely to be partially embedded into the surface, as shown by the middle particle, and some seem to rest on the surface, as shown by the schematic particle on the right.

Essentially, it would appear from the investigation of particle position, that any ballistic behavior for these largest of particles in the size range of interest is a weak phenomenon at best, or may not be occurring, at worst. This may not be the case for all potential target materials, but it seems to be true for low concentration gelatin.

5.3 – Comparison To Theory

A theoretical correlation between penetration depth and: particle radius, physical properties, and impact speed; was developed in Chapter 2, and can now be used to determine if the behavior observed from experimental data fits with this model. The model itself predicts the depth of the leading edge of the particle, so the experimental data must be shifted by the average radius of the particle for proper comparison with the model.

Since the theoretical equation uses measurable physical properties, it was decided to represent the predicted values for the average properties found, with dashed lines indicating the bounds of the predicted penetration using the physical properties at the appropriate edges of their uncertainty ranges. Thus, the lower range of penetration would correspond to lowest mean impact velocity, highest target density and tensile strength, while the upper range of penetration would correspond to the opposite extreme of these properties. The resulting prediction for this experiment is shown in Figure 5.4 below.

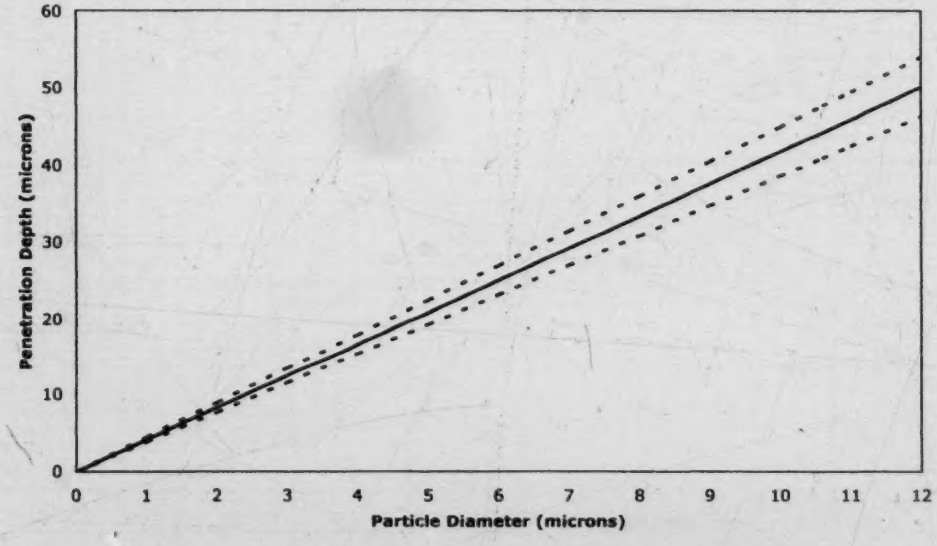

Figure 5.4: Predicted Range of Penetration for varying Physical Properties

As can be seen, for the 10.60 micron particles fired, the theory predicts a minimum penetration depth of approximately 41 microns for the particle leading edge. Considering that the particles appeared to penetrate to a maximum of 5.3 microns (i.e. the mean particle radius), it is therefore reasonable to say that this theory does not adequately predict the behavior of the particles penetrating into the gelatin.

5.3.1 – Possible Unconsidered Penetration Mechanisms

Since the theory is inadequate to describe what was seen in experiment, it would seem that there are two distinct possibilities: the behavior observed shows that aerosol particles will not behave in a ballistic fashion when impacting into gelatin; or that there are physical factors present which weakened the ballistic behavior severely.

The question then becomes: what physical mechanisms could there be, that were unaccounted for during theoretical considerations?

One such possibility is an effect that could be present due to the deformation of the gelatin surface by the air jet. Given that the gelatin specimen is constrained on all sides except the surface, there exists the potential for local compression of the gelatin. As such, this could potentially lead to a local increase in density, as the hydrolyzed proteins which gelatin is made up of are forced closer together. Such an increase in density would directly decrease the depth to which particles could penetrate. A local density increase might also increase the local yield strength of the target, as its molecules would be closer packed, and on a small scale might exhibit the characteristics of a higher concentration gelatin.

The extent to which such effects may play a role in impact behavior of deforming media is uncertain. While such a mechanism sounds feasible, the author is unaware of any studies into such phenomena.

Another mechanism that was left unconsidered in theory was that of frictional forces acting on a particle once it entered the gelatin material. Ballistic penetration theory assumes that such forces are negligible compared to the tensile force, and the target inertial resisting force, as a thin film of molten target material typically surrounds a projectile exhibiting ballistic behavior, and the fluid drag force is quite small.

However, the particle may have experienced significant forces relative to its size from fluid frictional forces. While a relatively small force might have negligible effect on a bullet with a mass of 50 g, the same force could have a much larger effect on a 10.6 micron particle whose mass is a mere $1x10^{-9}$ g.

Alternatively, a particle with such small mass and a relatively low velocity may not possess sufficient energy to melt surrounding target material as it passes into, and through the target. Instead, the particle may experience a frictional force due to the gelatin's elasticity causing it to attempt to close, pushing radially inward on the surface of the particle.

Finally, the theory did not take into account the elasticity of the gelatin. A particle impacting on the surface may in fact stretch the surface (creating a miniature depression) prior to rupturing the surface. If there was no way to return this potential to the particle upon rupture, such a stretching mechanism could potentially rob the particle of a significant amount of kinetic energy, and therefore, penetration velocity.

5.3.2 – Possible Amendments to Theory

A purely ballistic theory appears to be inadequate to model the behavior of aerosol particles impacting into a gelatin target. A theory that incorporates a frictional resisting force is not 'ballistic' by the conventional definition, but such a 'pseudo-ballistic' theory may be of some utility.

First, the possibility of the surface deforming beneath the particle prior to rupture deserves consideration. On a macro scale, it was observed that the gelatin could withstand large deformations under the high-pressure air jet without breaking. If a certain amount of surface displacement prior to rupture is assumed, one can determine the elastic energy stored by the gel prior to rupturing. Assuming a contact geometry as shown in Figure 5.5 below, the potential energy stored can be calculated if the gelatin is treated as having the properties of an infinite number of infinitesimal number of identical vertical springs.

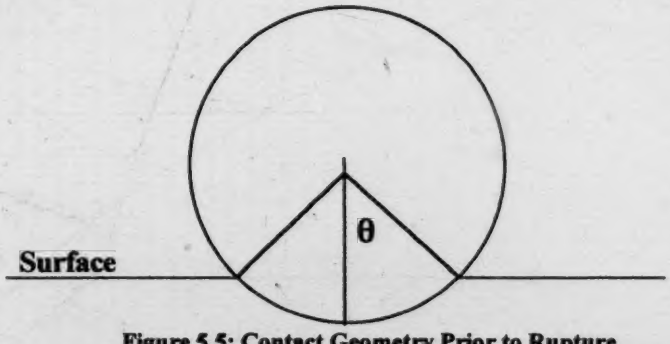

Figure 5.5: Contact Geometry Prior to Rupture

With this geometry, an equation total amount of energy stored prior to rupture was calculated to be

$$\frac{\pi}{16} k d^2 \left[6\theta - 8\sin\theta + \sin(2\theta) \right], \qquad (15)$$

where k is the effective spring constant of the gelatin, and d is the particle diameter.

Benmouna and Johannsmann (2004) measured an effective spring coefficient of $0.1 N/m$ for a low concentration gel. While the exact concentration of their gel is unknown due to it having been formed through evaporation, it was initially made from a 0.5% concentration gelatin solution. It therefore seems reasonable to use this spring constant value as a base estimate for the spring constant of the gelatin.

Recalling that the measured velocity of the particles must be multiplied by two factors to attempt to account for the particle slowing as it approaches the target, an average velocity of 25 m/s was used to estimate that a 10.6 micron particle would impact the surface with a kinetic energy of approximately $0.05886 \mu J$. The amount of energy that could be stored due to elastic deformation of the surface prior to rupture is summarized for a range of angles in Table 5.2 below. (A derivation of the equation leading to these theoretical values can be found in Appendix C.)

Table 5.2: Potential Elastic Energy Stored for a Given Contact Angle

Fraction of Pi	Stored Energy (J)
0	0.00E+00
1/6	1.68E-14
1/4	1.23E-13
1/3	4.88E-13
1/2	3.14E-12

Given that the largest of these values is four orders of magnitude smaller than the kinetic energy of the particle, it can be assumed that any energy stored elastically by the gelatin prior to rupture is negligible.

This approximation does not take into account the potential energy that could be stored by horizontal displacement, and may not be adequate to describe the total elasticity of the surface.

It is next beneficial to investigate the possible effects on the theoretical model of adding a frictional resistive force. Before a frictional resisting force can be added, it must be determined which type of force, fluid drag or surface-to-surface friction, is most likely to be present for an aerosol penetrating into a target.

In the case of gelatin, this requires for a simple analysis of the heat required to melt a small amount of gelatin surrounding the particle. It was assumed for the purposes of this calculation that the gelatin surrounding the particle within 0.5 microns of the particle surface would melt, providing the fluid to drag upon the particle.

The gelatin's heat capacity of 2 $Jg^{-1}K^{-1}$ and heat of melting of 40 J/g were estimated from the work of Tseretely and Smirnova (1992). It was calculated that the thermal energy required to raise the temperature of, and then melt, a 0.5 micron layer of gelatin surrounding a 10.6 micron particle with initial impact speed of 25 m/s, would be approximately 0.01964 μJ. (A detailed calculation of this can be found in Appendix C.)

This is nearly a full one third of the kinetic energy such a particle possesses, and temporarily melting this much gelatin would require the particle to reduce its velocity by roughly 40% immediately.

For a sphere traveling in a liquid medium, a drag force must be estimated. One such estimation is that of Stokes' drag. While Stokes' drag is most accurate for particle Reynolds numbers much smaller than one, the relative simplicity of the expression makes it attractive for possible inclusion in theory. If Stokes' drag is assumed to be acting on the particle, it adds a drag force of

$$F_D = 3\pi d_p \mu V, \qquad (16)$$

and the force it would give for a velocity reduced by 40% due to thermal dissipation would be eight orders of magnitude smaller than the next largest force acting upon the particle according to theory. Thus, the bulk of the effect of a small fluid film being formed around a particle would primarily be due to the dissipation of energy as heat to melt the surrounding gelatin.

Finally, the possibility of effects due to solid-solid contact between the gelatin and a particle was considered. In a similar fashion to the analysis employed for determining energy stored in a deforming surface, an estimate of the normal forces acting on a particle penetrating the gelatin (and therefore, the frictional force) was calculated. For a sphere, the total frictional force resisting the sphere's motion is

$$F_f = 2\pi k d_p \mu_k, \qquad (17)$$

where μ_k is the kinetic coefficient of friction in the material. While this friction of coefficient is unknown, the other terms are all known. Much like the fluid drag force, this frictional force (ignoring the friction coefficient) would be eight orders of magnitude smaller than the next largest resisting force considered in theory. Thus, the frictional force would also have a negligible effect on the theory.

If one incorporates the velocity loss due to locally melting the surrounding gelatin, the theoretical prediction for the mean speed measured for 10.60 micron particles drops to from 44.27 microns to 32.35 microns. While this is an improvement in accuracy, the predicted penetration it is still significantly different from the penetration observed.

Chapter 6

Conclusions and Recommendations

6.1 – Conclusions

Having completed a study of the interactions between aerosol particles fired in a jet of air into a gelatin target of known concentration, several conclusions can be drawn.

It was found that the behavior of the particles upon contact with the target did not agree with the theoretical model presented, and attempts to reconcile theory and experiment yielded limited results. Therefore, the behavior is not ballistic, or is an extremely weak 'pseudo-ballistic' behavior at most.

It is thought that much of the discrepancies may be a result of unforeseen physical mechanisms, which were not incorporated into the model originally. These may include local density and strength increases in the constrained gelatin sample due to compression from the air stream, as well as significant losses of kinetic energy to heating a small pocket of gelatin around the particle.

Overall, while the author is confident that there may still be a suitable target medium for ballistic collection of atmospheric aerosol in remote environments; gelatin is not a good candidate for this application.

With these conclusions in mind, there are several recommendations for future work that may be pursued in this area of study.

6.2 – Recommendations

In order to find a suitable medium, there are several suggested changes to both the experimental methodology, and the properties of a suitable material for ballistic testing.

With regards to experimental methodology, the first recommendation is to design a method of launching particles that does not rely upon entraining them into a stream of air. While air entrainment is convenient, cheap, and lightweight, if any suitable material found will elastically deform under application of an air jet there may be significant velocity losses prior to particle impact which would reduce the efficacy of such a size-sampling device. One possible replacement method for particle firing is that of a high speed piston 'ram', which would rely upon a physical carrier to accelerate the particles, and is shown in a conceptual schematic in Figure 6.1 below.

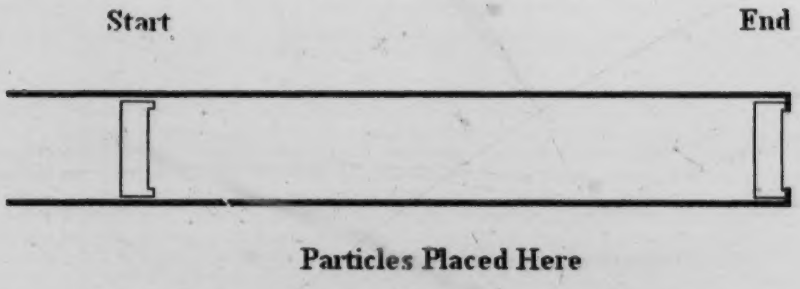

Figure 6.1: Schematic of a Piston Ram Particle Firing System

As shown in the schematic, a piston carrying a particle payload could be accelerated down a tube using air pressure; perhaps a burst diaphragm would break open upstream of the piston head, leading to a high pressure drop across the piston head. The end of the tube would have a narrower diameter than the piston head, and therefore would stop the piston head. The unconstrained particles riding on the piston surface, however, would continue forward due to the momentum imparted by the piston.

Such a system could be designed to operate in a horizontal manner if the area holding the particles were designed properly; however such a system may suffer a disadvantage of needing to be quite large and heavy.

In addition to a new method for particle firing, it is recommended that a vacuum chamber that is usable with a wide range of velocity measurement equipment be constructed for testing within. In ambient atmosphere, the piston head would build up a pressure wave that could have an effect on a test medium similar to the effect of a jet of air; operating in a vacuum would avoid this potential effect. Additionally, the use of a vacuum chamber could be used to model lunar or Martian ambient conditions between the particle firing device, and the target material.

Regarding material selection for the target, recommendations are more difficult to make. While achieving sufficiently high velocities in a vacuum may get the desired behavior with low concentration gelatin, such an apparatus would likely have to be large and heavy in order to be handle the pressure requirements of a piston-style firing mechanism. There may be other materials that could provide the desired type of behavior; perhaps a foam of some type, or some type of soft, non-porous medium. In general, such a material would need to fracture on a micro scale at relatively low energies, but would need to deform as little as possible if used in ambient air, or with an air jet.

The author believes that following the recommendations above could eventually lead to a device capable of traveling to distant and hard to reach locales, and size atmospheric aerosol, or aerosol sized dust collected from the surface of the area.

Bibliography

Anderson, S.L., and Longmire, E.K. (1995) Particle Motion in the Stagnation Zone of an Impinging Air Jet, *Journal of Fluid Mechanics* 299:363-366

Awerbuch, J. (1970) A mechanics approach to projection penetration, *Israel Journal of Technology* 8: 375-383

Benmouna, F. and Diethelm Johnnsmann (2004) Viscoelasticity of Gelatin Surfaces Probed by AFM Noise Analysis, *Langmuir* 20:188-193

Burwash, W., Finlay, W.H., and Matida, E. (2006) Deposition of Particles by a Confined Impinging Jet onto a Flat Surface, *Aerosol Science and Technology* 40:147-156

Dehn, J. (1987) A unified theory of penetration, *International Journal of Impact Engineering* 5:239-248

Fairweather, M. and Hargrave, G.K. (2002) Experimental investigation of an axisymmetric, impinging turbulent jet. 1. Velocity field, *Experiments in Fluids* 33: 464-471

Finlay, W.H. *The Mechanics of Inhaled Pharmaceutical Aerosols*, Academic Press, London, UK. (2001) pg. 27

Groot, R.D., Bot, A. and Agterof, W.G.M. (1996) Molecular theory of strain hardening of a polymer gel: Application to gelatin, *Journal of Chemical Physics* 104:9202-9219

Hardy, M.P. and Kendall, M.A.F (2005) Mucosal deformation from an impinging transonic gas jet and the ballistic impact of microparticles, *Physics in Medicine and Biology* 50:4567-4580

Mars General Circulation Modeling Group at NASA Ames, *Is there liquid water on Mars?* http://www-mgcm.arc.nasa.gov/mgm/HMTL/FAQS/liquid.html, 2004. Last visited on 13 October, 2006

Mitchell, T.J., Kendall, M.A.F., and Bellhouse, B.J. (2003) A ballistic study of micro-particle penetration into the oral mucosa, *International Journal of Impact Engineering* 28:581-599

Rao, N.P., Navascues, J. and Fernandez de la Mora, J. (1993) Aerodynamic focusing of particles in viscous jets, *Journal of Aerosol Science* 24:879-892

Tseretely, G.I., and Smirnova, O.I. (1992) DSC Study of melting and glass transition in gelatins, *Journal of Thermal Analysis* 38:1189-1201

Wang, Z.L., Grgic, B, and Finlay, W.H. (2006) A Dry Powder Inhaler with Reduced Mouth-Throat Deposition, *Journal of Aerosol Medicine* 19:168-174

Appendix A

MAT Lab Image Processing Code

```
%This is an image processing program which determines
particle penetration depth.
%This Program Is Modified Each time it is run to process an
array of images, and return
%the image locations (optical sectioning planes) where each
particle detected is
%largest and brightest.  (And therefore is the midplane of
the particle)
clear

%Array of Names of Images to be processed
initial = {'img.tif' 'img(1).tif' 'img(2).tif' 'img(3).tif'
'img(4).tif' 'img(5).tif' 'img(6).tif' 'img(7).tif'
'img(8).tif' 'img(9).tif' 'img(10).tif' 'img(11).tif'
'img(12).tif' 'img(13).tif' 'img(14).tif' 'img(15).tif'
'img(16).tif' 'img(17).tif' 'img(18).tif' 'img(19).tif'
'img(20).tif' 'img(21).tif' 'img(22).tif' 'img(23).tif'
'img(24).tif' 'img(25).tif' 'img(26).tif' 'img(27).tif'
'img(28).tif' 'img(29).tif' 'img(30).tif' 'img(31).tif'
'img(32).tif' 'img(33).tif' 'img(34).tif' 'img(35).tif'
'img(36).tif' 'img(37).tif' 'img(38).tif' 'img(39).tif'
'img(40).tif' 'img(41).tif' 'img(42).tif' 'img(43).tif'
'img(44).tif' 'img(45).tif' 'img(46).tif' 'img(47).tif'
'img(48).tif' 'img(49).tif' 'img(50).tif' 'img(51).tif'
'img(52).tif' 'img(53).tif' 'img(54).tif' 'img(55).tif'
'img(56).tif' 'img(57).tif' 'img(58).tif' 'img(59).tif'
'img(60).tif' 'img(61).tif' 'img(62).tif' 'img(63).tif'
'img(64).tif' 'img(65).tif' 'img(66).tif' 'img(67).tif'
'img(68).tif' 'img(69).tif' 'img(70).tif'};

%input outer loop size = number of images to be processed
index = 66;
%create an array to store number of particles at midplane
in each image
largeparts = zeros(250,index);
smallparts = zeros(250,index);
%Minimum and Maximum Radius of Particles to be considered
(px)%
```

```
%Values should be [meanrad(min/max)]: 10.60(3.5/3.7),
7.09(2.3/2.5), 3.16(1.0/1.15)
minsize = 2.5;
maxsize = 6.0;
sminsize = 1.0;
smaxsize = 1.15;
%cutoff for black & white filter
bwcutoff = 0.5;

%----------------Start of Image Processing----------------
---------------%

%begin outer loop
for i = 1:index;

imgnm = initial(i);
imgname = char(imgnm);
image = imread(imgname);
%convert image to double format%
gimg = im2double(image);

%top-hat filter the image (filters out large clumps of
particles)%
se = strel('disk', 6);
topimg = imtophat(gimg, se);

%To reduce noise, convert to B&W image with a threshold of
0.5%
bwimg = im2bw(topimg, bwcutoff);

%Number particles with bwlabel%
[L,NUM] = bwlabel(bwimg);
gbwimg = im2double(bwimg);
%array multiply tophat with bw image to cut noise out of
the tophat picture%
ntopim = topimg .* gbwimg;

%find the average intensity of each particle by averaging
the intensity of each pixel%
brtary = zeros(2,NUM);
for ctr = 1:NUM
    %find coordinates of each pixel in particle
    [xcor,ycor] = find(L == ctr);
    %count number of pixels in each particle%
    [numr,numc] = size(xcor);
    %store area of particle in px%
    brtary(2,ctr) = numr;
```

```
    for ct2 = 1:numr
        %sum intensities of each pixel in each particle%
        brtary(1,ctr) = brtary(1,ctr) +
ntopim(xcor(ct2),yc r(ct2));
    end
    %divide by number of pixels in particle to get avg
intensity%
    brtary(1,ctr) = brtary(1,ctr) / brtary(2,ctr);
end

%----------particle radius distribution----------%

rad = zeros(NUM,1);
% assume all particles are roughly circular %
for ct4 = 1:NUM
    rad(ct4) = sqrt(brtary(2,ct4) / pi);
end

%-------Filter Filter Particles by size, dump into global
data array------%

tempind = 1;
for ct5 = 1:NUM
    if rad(ct5) >= minsize
        if rad(ct5) <= maxsize
            largeparts(tempind,i) = brtary(1,ct5);
            tempind = tempind + 1;
        else
        end
    else
    end
end

tempind = 1;
for ct5 = 1:NUM
    if rad(ct5) >= sminsize
        if rad(ct5) <= smaxsize
            smallparts(tempind,i) = brtary(1,ct5);
            tempind = tempind + 1;
        else
        end
    else
    end
end

%print index of image completed, just to show program
hasn't frozen
```

```
%remove this after debugging
i

%end outer loop
end

%--------------------End of Image Processing----------------
------%

%-------Process Global Array to find max brightness values-
------%
brightest = 0;
sbrightest = 0;
for ct6 = 1:index
    for ct7 = 1:250
        if largeparts(ct7,ct6) > brightest
            brightest = largeparts(ct7,ct6);
        else
        end
        if smallparts(ct7,ct6) > sbrightest
            sbrightest = smallparts(ct7,ct6);
        else
        end
    end
end

%--------Find all particles in max brightness range--------
-----%

%set lower limit for brightness
minbright = 0.90 * brightest;
sminbright = 0.90 * sbrightest;

%initialize array to store number of midplane particles in
each section
nummidpart = zeros(index,1);
snummidpart = zeros(index,1);

%count number of midplane particles in each section
for ct8 = 1:index
    for ct9 = 1:250
        if largeparts(ct9,ct8) >= minbright
            nummidpart(ct8) = nummidpart(ct8) + 1;
        else
        end
        if smallparts(ct9,ct8) >= sminbright
            snummidpart(ct8) = snummidpart(ct8) + 1;
```

```
        else
        end
    end
end

%for checking purposes, count total number of particles at
brightest
totalparticles = 0;
for ct10 = 1:index
    totalparticles = totalparticles + nummidpart(ct10);
end
%Display total particles
totalparticles

%----------------Plot Particle Distribution----------------
--%

%write an x-coordinate array, by picture number
X = zeros(index,1);
xtemp = 0;
for ct11 = 1:index
    X(ct11) = xtemp;
    xtemp = xtemp + 1;
end
figure, plot(X,nummidpart,'b-o',X,snummidpart,'r-+');
title('Number of Particles whose depth is in each image')
xlabel('Image Number');
ylabel('Number of Particles');
```

Appendix B

Raw Data

Velocity Measurements

Table B.1: Velocity Measurements Taken with LDA

Experiment	V_{mean} (m/s)	ΔV_{RMS} (m/s)	# Att. Samp.	% Accepted	% Spherical
LPE 5	66.630	5.994	192.000	46.350	24.700
LPE 6	72.640	4.462	144.000	50.000	40.200
LPE 7	70.670	5.871	240.000	87.080	42.100
LPE 8	71.990	3.505	112.000	73.210	36.500
LPE 9	63.600	2.745	208.000	78.360	28.800
LPX 1	62.760	3.671	64.000	73.430	51.000
LPX 2	68.550	9.829	183.000	74.310	55.700
LPX 4	66.900	6.973	64.000	78.120	32.000
LPX 5	70.380	9.890	80.000	62.500	38.000
LPX 6	67.747	6.001	239.000	66.527	31.496
Average	68.187	5.894	152.600	68.989	38.050
Stand. Dev.	3.3361	2.4778	69.3961	12.8478	9.6953

Graphical Output For Experiments Yielding Valid Penetration Results

Experiment LPV3:

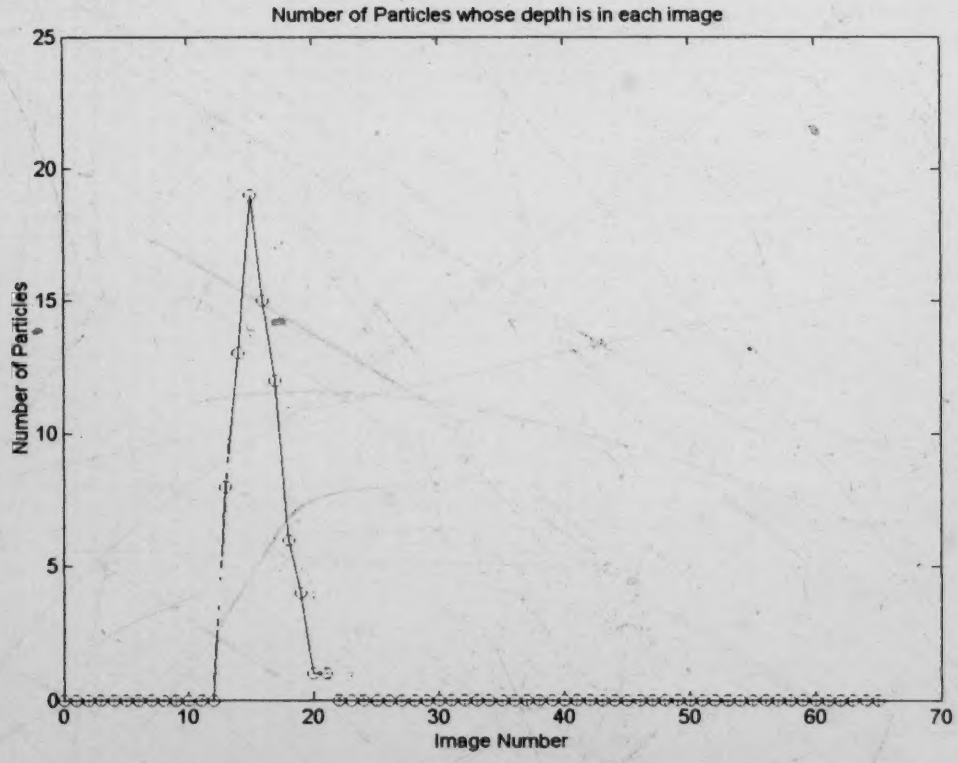

Figure B.1: Graphical Output for Penetration Depths of Experiment LPV3

Experiment LPV4:

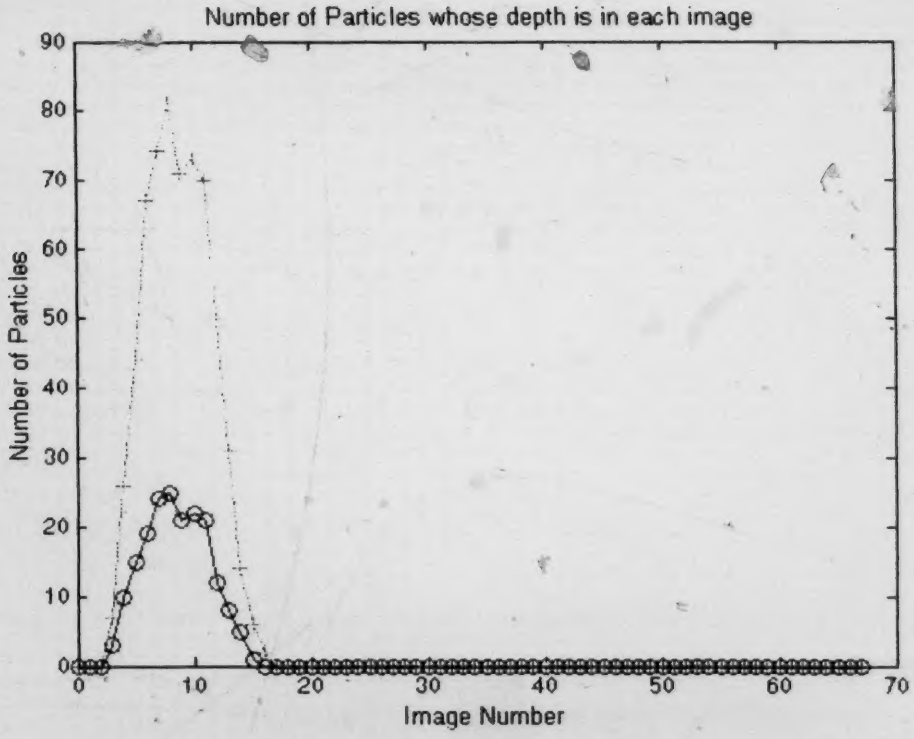

Figure B.2: Graphical Output for Penetration Depths of Experiment LPV4

Table B.2: Penetration Depth Data Taken From Program Output

	LPV3				LPV4			
Image #	# Small	# Large	# Sm*Img	#Lg*Im	# Small	# Large	# Sm*Img	#Lg*Im
0	0	0	0	0	0	0	0	0
1	0	0	0	0	0	0	0	0
2	0	0	0	0	0	0	0	0
3	1	0	3	0	7	3	21	9
4	7	8	28	32	26	10	104	40
5	19	13	95	65	44	15	220	75
6	21	19	126	114	67	19	402	114
7	22	15	154	105	75	24	525	168
8	17	12	136	96	81	25	648	200
9	11	6	99	54	71	21	639	189
10	5	4	50	40	74	22	740	220
11	4	1	44	11	70	21	770	231
12	1	1	12	12	50	12	600	144
13	0	0	0	0	31	8	403	104
14	1	0	14	0	14	4	196	56
15	0	0	0	0	5	1	75	15
16	0	0	0	0	2	0	32	0
17	0	0	0	0	0	0	0	0
18	0	0	0	0	0	0	0	0
19	0	0	0	0	0	0	0	0
20	0	0	0	0	0	0	0	0
	Sm. Mean Img Loc	6.982			Sm. Mean Img Loc	8.712		
	Lg.Mean Img. Loc	6.696			Lg.Mean Img. Loc	8.459		
	Depth(μm)	0.285			Depth(μm)	0.252		

Appendix C

Derivations

C.1 – Stored Elastic Energy Due to Surface Deformation

Begin by examining the schematic presented in chapter 5, for a particle pressing into the gelatin surface.

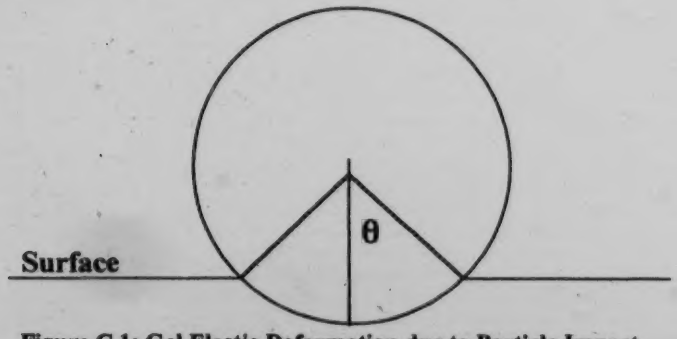

Figure C.1: Gel Elastic Deformation due to Particle Impact

The depth any part of the surface is deformed to is equal to the difference between the particle radius, and the distance between the undeformed surface location, and the particle center:

$$s = r - r\cos\theta. \tag{C.1}$$

Assume that any infinitesimal cross section of the gelatin behaves as a spring. The energy stored in a spring is given as

$$U = \frac{1}{2}ks^2. \tag{C.2}$$

Therefore, if the energy stored is integrated over the area that is depressed by the particle prior to rupture, this will yield the total energy stored prior to rupture.

Substituting C.1 into C.2 and integrating over the two angles defining contact, the integrand is expressed as

$$U = \int_0^{2\pi}\int_0^{\theta}\frac{1}{2}k(r - r\cos t)^2\,dt\,d\varphi \qquad \text{(C.3)}$$

C.3 may be expanded and simplified to

$$U = \int_0^{2\pi}\int_0^{\theta}\frac{1}{2}kr^2(1 - 2\cos t + \cos^2 t)\,dt\,d\varphi \qquad \text{(C.4)}$$

Integrating C.4 and substituting *d/2* for *r* yields the final form of

$$U = \frac{\pi}{16}kd_p{}^2[6\theta - 8\sin\theta + \sin(2\theta)]. \qquad \text{(C.5)}$$

C.2 – Frictional Force Acting on a Spherical Particle

In a similar fashion to the analysis of surface deformation of energy, it is possible to derive the frictional force acting upon a particle passing through a consistent medium.

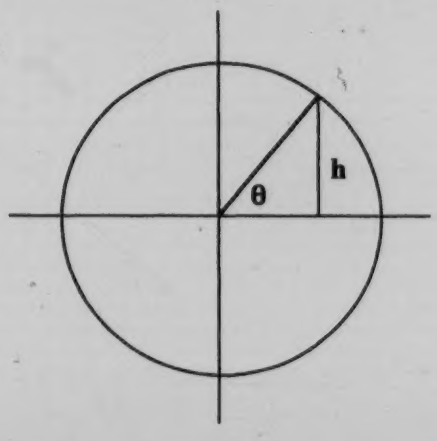

Figure C.2: Particle Schematic for Frictional Force Derivation

In this case, the amount which any single differential 'element' of the gelatin is deformed, h, is defined as

$$h = r\sin\theta. \qquad \text{(C.6)}$$

Assuming again that each 'element' behaves as a spring, the normal force acting on a single particle is

$$F = kh, \tag{C.7}$$

or,

$$F = kr\sin\theta. \tag{C.8}$$

Therefore, given symmetry considerations, the total normal force acting on one half the particle is

$$F_N = \int_0^{2\pi}\int_0^{\pi/2} kr\sin\theta d\theta d\varphi. \tag{C.9}$$

Integrating, this yields a normal force of

$$F_N = 2\pi kr. \tag{C.10}$$

Recognizing that the frictional force is simply this normal force times a coefficient of kinetic friction, it becomes a trivial matter to substitute in diameter and multiply by two to account for friction on both sides of the particle. This yields a final expression for the frictional force acting on a spherical particle of:

$$F_f = 2\pi k d_p \mu_k. \tag{C.11}$$